Geomorphology 511 (2026) 110414

Contents lists available at ScienceDirect

Geomorphology

journal homepage: www.journals.elsevier.com/geomorphology

Geomorphological and hydrological controls on shallow karst depressions (dayas) on a planar carbonate platform: the Nullarbor Plain, Australia

Matej Jelovčan [a,*], Uroš Stepišnik [b], Andrej Šmuc [c], Primož Miklavc [c], Matej Dolenec [c], Matej Lipar [d]

[a] Karst Research Institute, Research Centre of the Slovenian Academy of Sciences and Arts, Postojna, 6230, Slovenia
[b] Department of Geography, University of Ljubljana, Ljubljana, 1000, Slovenia
[c] Department of Geology, Faculty of Natural Sciences and Engineering, University of Ljubljana, Ljubljana, 1000, Slovenia
[d] Anton Melik Geographical Institute, Research Centre of the Slovenian Academy of Sciences and Arts, Ljubljana, 1000, Slovenia

ARTICLE INFO

Keywords:
Dayas
Doline
Geomorphology
Hydrology
Sedimentology
Arid karst
GIS
Nullarbor Plain

ABSTRACT

Dayas are shallow karst depressions that represent one of the most widespread surface landforms in arid karst environments, where present-day dry climatic conditions strongly limit karstification processes. This paper provides a comprehensive geomorphological analysis of dayas on the Nullarbor Plain in southern Australia, one of the world's largest exposed carbonate platforms and an ideal natural laboratory due to its tectonic stability and lack of orogenesis. Semi-automatic GIS-based detection and morphometric analysis were conducted across 11 representative study areas (300 km^2 each), complemented by sedimentological analyses (grain-size distribution and XRD). In addition, a GIS-based assessment of water retention in inundated dayas following an extreme flood event in March 2024 was performed by comparing theoretical evaporation losses and observed changes in water volume, supported by meteorological data. Our results demonstrate that palaeotopography exerts a strong control on the spatial distribution and morphometric characteristics of dayas. Additionally, sedimentological analyses indicate a poorly permeable sediment infill resulting from aeolian and fluvial accumulation and reworking, which promotes prolonged surface-water retention within the depressions. Discrepancies between observed water-volume losses and theoretical evaporation indicate partial floodwater infiltration into the karst aquifer, suggesting that dayas may act as focused, event-based recharge features and are not solely relict landforms, but rare surface karst features that remain active under present arid conditions. These findings mark the first application of an integrated methodological approach to the study of dayas and yields new insights into their spatial evolution and geomorphological and hydrological significance on planar carbonate platforms such as the Nullarbor Plain, while offering a framework applicable to analogous arid karst regions worldwide.

1. Introduction

Arid and semi-arid landscapes, which occupy one third of the Earth's land surface (Wickens, 1998), are characterised by low precipitation, high evapotranspiration and geomorphic systems dominated by limited but episodic surface run-off and often extensive wind reworking. Where soluble rocks are present, karst geomorphology may also develop, but its present expression is generally weak and strongly limited by low rainfall. Many preserved landforms are relict features that developed during past periods of wetter climatic conditions when karstification was more effective (De Waele and Gutiérrez, 2022; Ford and Williams, 2007; Jennings, 1983; Salomon and Pulina, 2005; Webb and White, 2013).

The characteristic landforms of arid karst are shallow sediment-infilled circular to subcircular depressions formed in carbonate bedrock termed dayas, commonly regarded as a subtype of solution dolines (Capot-Rey, 1939; Castellani and Dragoni, 1977, 1986; Clarke et al., 1974; Gautier, 1951; Goudie, 2010; Mitchell, 1970; Mitchell and Willimott, 1974). Although locally referred to by varying terms (e.g., balte, vleis, chor/sor, dongas), the term “dayas” from northwestern Africa has become the standard descriptor in geomorphological literature (Agabi, 1995; Clarke et al., 1974; Goudie, 2010; Jennings, 1983). In contrast, other closed depressions in arid environments, such as clay pans, are widespread in non-carbonate settings and are primarily controlled by deflation, salt weathering, and disruption of drainage

* Corresponding author.
E-mail address: matej.jelovcan@zrc-sazu.si (M. Jelovčan).

https://doi.org/10.1016/j.geomorph.2026.110414
Received 3 March 2026; Received in revised form 21 May 2026; Accepted 9 June 2026
Available online 11 June 2026

systems rather than dissolution of bedrock (Goudie, 1991).

Dayas span several tens of metres to several kilometres in diameter, while even the largest rarely exceed 10 m in depth (Castellani and Dragoni, 1977; Clarke et al., 1974; Goudie, 2010; Mitchell, 1970; Mitchell and Willimott, 1974). Following high-intensity rainfall events, dayas may host ephemeral lakes (Capot-Rey, 1939; Clarke et al., 1974; Gautier, 1951; Mitchell, 1970; Mitchell and Willimott, 1974). Their higher soil moisture supports vegetation and localised wetland ecosystems (Babikir, 1986; Thiéry, 1991), and they may be used for cultivation and grazing (Goudie, 2010; Mitchell and Willimott, 1974).

The basic genetic mechanism of bedrock dissolution can be accompanied by additional modification processes, e.g. aeolian modification, interactions with fossil or active drainage networks and with sand-dune systems (Capot-Rey, 1939; Clarke et al., 1974; Conrad et al., 1967; Goudie, 2010; Mabbutt, 1977; Mitchell, 1970; Mitchell and Willimott, 1974). Their fine-grained infill reflects alluvial and aeolian deposition, as well as pedogenesis (Mitchell and Willimott, 1974). Early classifications emphasised morphology and drainage context (Castellani and Dragoni, 1977; Clarke et al., 1974), whereas Goudie (2010) later proposed a typology based on global morphogenetic/morphological traits. This typology distinguishes between simple circular type, regarded as the classic daya, the centripetal type with converging inflow channels, the structurally controlled type, governed by bedrock discontinuities (e.g., joints, fractures, bedding planes), the drainage channel type developed within palaeochannels, and the wind aligned type, which is linked to the presence of active or relict dune systems.

Despite their common occurrence, dayas remain comparatively underrepresented in arid karst research, in part because their shallow expression makes systematic detection challenging (Goudie, 2010). Most detailed studies date from the mid- to late twentieth century and focus on development, morphology and sedimentary infill, largely in the north-western Sahara (Castellani and Dragoni, 1977, 1986; Clarke et al., 1974; Conrad et al., 1967; Mabbutt, 1977; Mitchell, 1970; Mitchell and Willimott, 1974). A smaller but growing number of recent investigations have applied automated or semi-automated GIS-based detection approaches (Doerr and Davies, 2007; Goudie, 2010; Moussaoui et al., 2024; Tanh, 2021). However, comparatively few studies have explicitly examined whether dayas currently permit infiltration or whether floodwaters predominantly evaporate, even though this distinction is central to evaluating whether these features function as active components of the hydrological system or represent largely relict forms.

The Nullarbor Plain in southern Australia provides an ideal natural laboratory in which to address these uncertainties. As a passive continental margin and unaffected by orogenesis, it offers a laterally extensive surface approximately 700 km east–west and 300 km north–south. In this paper, we present a comprehensive analysis of dayas across the Nullarbor Plain. We identified over 150,000 shallow closed depressions using semi-automatic remote sensing, obtained quantitative morphometric descriptors, analysed sediment samples, and assessed flood-water retention following the major floods of March 2024 in order to determine whether these landforms currently function as infiltration features or whether they primarily retain water until it all evaporates. Our aim is to evaluate their spatial distribution and hydrological behaviour across the Nullarbor Plain in relation to topography. This integrated approach provides a representative and analytically robust assessment of dayas in an arid karst environment and contributes to a broader understanding of daya morphometric characteristics and the geomorphic evolution of the region.

2. Regional setting

The Nullarbor Plain forms the largest exposed karst surface in Australia and one of the largest globally, extending across ~200,000 km^2 on the border of Western Australia and South Australia (Delisser, 1865; Lowry and Jennings, 1974; Webb and James, 2023), terminating in the south as one of the longest clifflines in Australia along the Great Australian Bight (Wakelin-King and Webb, 2020). Geologically, it represents a broad, well-preserved carbonate platform of the Eucla Basin composed of horizontally bedded Eocene–Miocene limestones (Benbow et al., 1995; Lowry, 1970; O'Connell et al., 2012).

The carbonate units of the Eucla Basin are (in stratigraphic order): a) Middle to Late Eocene Wilson Bluff Limestone (maximum thickness of 300 m) is a soft, poorly lithified, muddy to chalky bryozoan-rich cool-water carbonate (Benbow et al., 1995; James and Bone, 1991; Playford et al., 1975); b) Oligocene to early Miocene Abrakurrie Limestone (maximum thickness 100 m) that is a granular neritic, bryozoan-rich, cool-water carbonate (Benbow et al., 1995; James and Bone, 1991; Li et al., 1996; Playford et al., 1975); c) middle Miocene Nullarbor Limestone (maximum thickness 45 m) represented by a fossiliferous subtropical carbonate forming the present-day plateau surface (Benbow et al., 1995; Hocking, 1990; Lowry, 1970; Lowry and Jennings, 1974; O'Connell et al., 2012). To the north the topography transitions into large and extensive basin-like feature, characterised by Colville Sandstone and overlain by a variety of Quaternary deposits (Lowry, 1970). Similar basin-like feature occurs to the west, whilst to the east, there is a narrow coastal terrigenous clastic unit named the Yarle Sandstone (Benbow et al., 1995), in places overlain by longitudinal dunes.

A major Late Miocene eustatic fall (~14 Ma), combined with subsequent uplift, progressively exposed the Nullarbor Limestone (Gillieson and Spate, 1992; Hou et al., 2008; Lowry and Jennings, 1974; Sandiford, 2007). Limited to the southern low-lying Roe and Israelite Plains, a poorly cemented molluscan calcarenite, known as the Roe Calcarenite, was deposited during Pliocene high sea-level stands (James et al., 2006). Holocene stratigraphy is mainly represented on the margins of the plain as aeolian and beach quartz carbonate sand (Stewart et al., 2008; Short et al., 2024). The modern upper surface of the Nullarbor Limestone is widely indurated by pedogenic calcrete, locally several metres thick; this calcrete is mainly Pliocene–Pleistocene in age (Abeysinghe, 1998; Miller et al., 2012).

Denudation rates are low with estimated 30–60 m of surface removal over 14 Ma years of exposure (O'Connell et al., 2012; Stone et al., 1994). Slightly higher values occur in the coastal belt, where Nullarbor Limestone has been removed, exposing older Abrakurrie Limestone (Lowry and Jennings, 1974).

The relief of the Nullarbor Plain rarely exceeds 10 m, but exhibits considerable micro-scale geomorphic variability. The region preserves extensive relict longitudinal dune topography, which was imprinted into the Nullarbor Limestone, expressed today as ridge and swale topography (Burnett et al., 2020). Dayas are the dominant type of closed depression across the plain, whereas collapse dolines are less common, distinctly smaller in diameter and deeper, and occur mainly within ~60 km of the coast (Jennings, 1962; Lowry and Jennings, 1974; Webb and James, 2023). The region contains an exceptional density of blowholes (estimated between 10,000 and 100,000) which are narrow, sub-circular vertical solutional shafts with a diameter of 1–2 m and reaching depths of up to ~50 m (Burnett et al., 2013). Horizontal caves tend to be joint-controlled and exhibit limited active dissolution under modern arid conditions (Jennings, 1962; Webb et al., 2003; Webb and James, 2023).

Relict drainage channels occur across the western, northern and eastern margins of the plain. These shallow palaeochannels indicate former allogenic streams sourced from the Precambrian uplands and the Great Victoria Desert that infiltrated underground or evaporated before reaching the coast (Lowry and Jennings, 1974). These systems likely remained active into the Pliocene under wetter climates (Alley et al., 1999). In addition, pocket valleys incise the Wylie and Hampton Scarps by up to 500 m, with associated talus fans formed during wetter conditions (Lipar and Ferk, 2015).

3. Data and methods

3.1. Semi-automated detection

A semi-automated detection of closed depressions was undertaken across the Nullarbor Plain. The Nullarbor Limestone forms the dominant surficial lithology across the plain and is therefore the most relevant unit for understanding present-day karst morphology and the development of dayas. The younger coastal erosional plains (Israelite and Roe Plains), northern and western marginal basin-like depressions, and eastern marginal part overlain by longitudinal dunes differ geologically from the central plateau and were therefore excluded from the study. Interior study boundaries were defined using Eucla Basin lithostratigraphy and topographic discontinuities interpreted from shaded-relief and coloured-relief mapping.

The workflow was implemented in ArcGIS Pro 3.4 and QGIS 3.38, following the method developed by Mazej (2024) for identifying convex hills and uvalas using the topographic openness index (ITO) and the outermost closed contour method. While the true outline of a depression is expressed by changes in slope, often gradual and spatially variable in threshold, such delineation is difficult to automate; therefore, the outermost closed contour provides a sufficiently robust approximation. A combination of TanDEM-X digital elevation models (Digital Surface Model (DSM); 1.0 and 0.2 arc-second resolution and TanDEM-X EDEM (Edited Digital Elevation Model) was obtained from the German Aerospace Center (DLR) (EOC Geoservice, 2023; Wessel, 2018). As the models capture both land surface and above-ground objects such as vegetation, their performance is well suited to the non-urbanised conditions of the Nullarbor Plain characterised by low vegetation cover.

The TanDEM-X resolution was aggregated to 30 m, after which the DEM was smoothed using Focal Statistics with a 30 m radius. Resolution reduction and smoothing diminished noise and lessened the influence of small-scale topography during detection of depressions. To enhance the identification of shallow closed depressions, the DEM was vertically exaggerated by a factor of 100. In QGIS, the Relief Visualization Toolbox (Kokalj and Somrak, 2019) was applied to generate positive and negative topographic openness (ITO). Default parameters were limited to a 300 m neighbourhood and eight azimuthal directions. Depressions were defined where ITO values were < 30. This threshold was calibrated using visualisations and satellite imagery on selected areas.

Because the layer of topographic lows encompassed all types of depressions, the last-closed-contour method was applied to delineate the closed depressions contained within it. Owing to the size of the area, the study region was subdivided into 30 sections, which overlapped to reduce boundary errors. For each section, 5-m contour intervals were generated and closed contours lying within topographic-low polygons were selected. These contour lines were converted to polygons and merged into a single polygon layer. This method also merged convex features within dayas caused by aeolian sediment infill or denser patches of shrubs or trees that were not initially classified as topographical lows. Adjacent dayas with connecting floors were mapped as a single form.

Furthermore, detailed identification and analysis was carried out

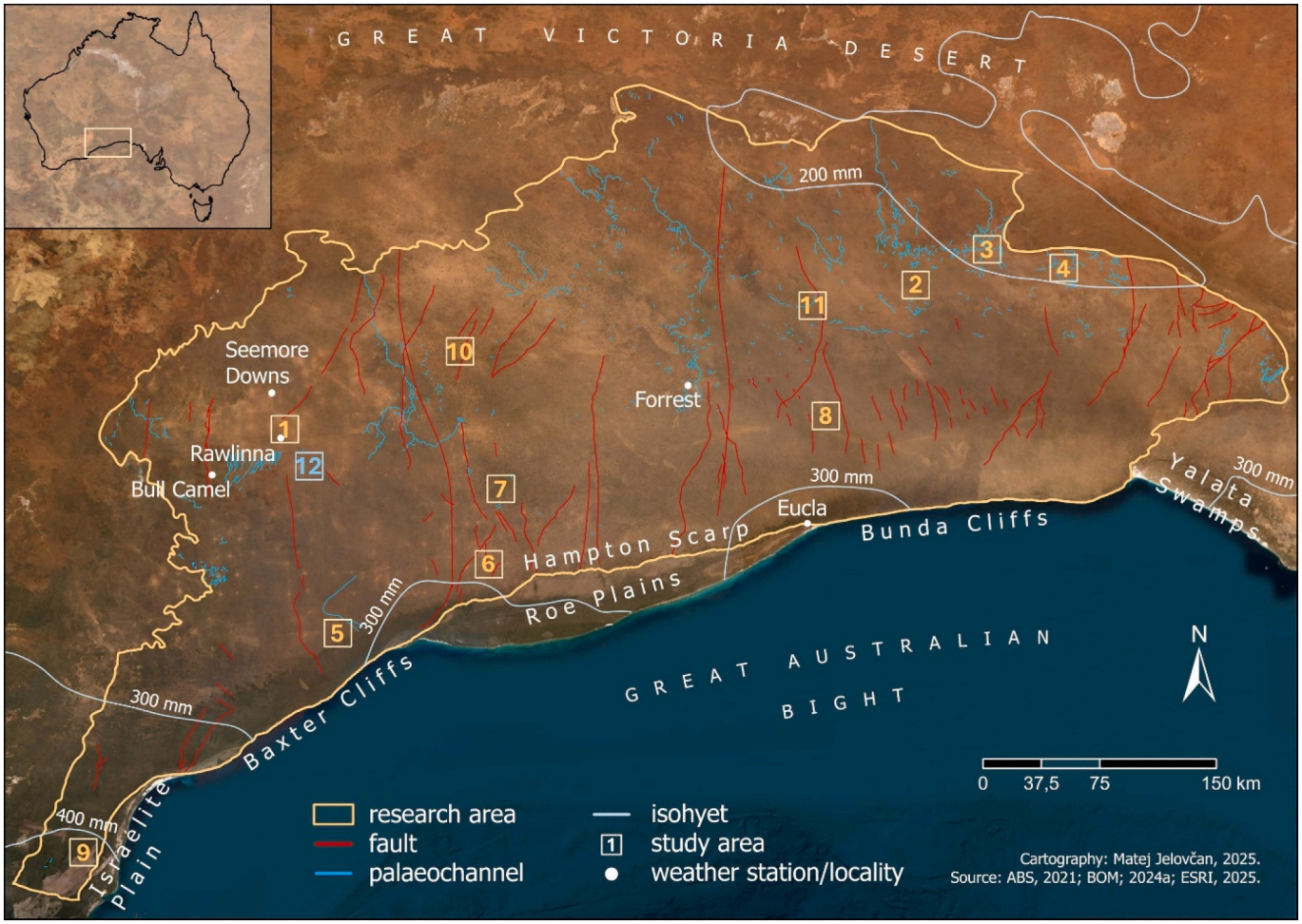

Fig. 1. Locality map showing study areas, major faults and palaeofluvial channels (identified from TandemX data). Areas 1–11 were selected for the analysis of morphological and morphometric characteristics of dayas, while Area 12 was used to study inundated dayas. Basemap and spatial data sources: ABS, 2021; BOM, 2024a; ESRI, 2025.

within selected representative areas, where additional datasets were used to refine interpretation and capture features that the automated procedure could not recognise. The closed depressions layer was therefore refined within 11 selected 300 km^2 control areas (see Fig. 1). These areas, including their number, size, and spatial distribution, were selected to capture the range and diversity of principal geomorphological settings of the Nullarbor Plain, namely drainage-controlled palaeochannels, ridge and swale topography terrains and planar surfaces (see Table 1, Figs. 4 and 5), and to enable their comparison. A regular, rectangular geometry was adopted as a practical and standard approach for defining large spatial sampling units guided by landscape variability, scale, and process heterogeneity (e.g., Goudie, 2004; Wilson and Gallant, 2000).

Verification and corrections within these areas relied also on radiometric satellite maps and surface-visualisation techniques. Potassium-Uranium-Thorium radiometric images and Advanced Spaceborne Thermal Emission and Reflection Radiometer (ASTER) images were obtained from the Commonwealth of Australia (Geoscience Australia, 2021). In radiometric imagery, contrasts between sediment-covered surfaces and exposed limestone appear as distinct boundaries. These differences reflect greater sediment accumulation and thus higher radiometric intensity within sediment-filled depressions, compared with rocky ridges where values are lower. Additional visualisation techniques included Color Relief Image Maps (CRIM). Combined depressions were retained where CRIM indicated a shared floor or indistinct slope transitions. The smallest dayas, often omitted due to the reduced resolution, were manually added in study areas based on visualisations and high-quality satellite imagery. This may introduce some morphometric bias due to possible inconsistencies in visual delineation across the study area, but the inclusion of small dayas (around 5000 m^2 or less) in the analysis is considered to outweigh the potential inaccuracies of manual detection. Moreover, blowholes and collapse dolines were excluded from manual mapping due to their significantly smaller size.

3.2. Morphometric analysis

Morphometric analysis involved the calculation of six parameters for each study area: surface area (m^2), perimeter length (m), circularity index, diameter (m), depth (m), and orientation (°). The circularity index was derived from surface area and perimeter length to quantify the degree to which the planform geometry of each polygon approaches a circular shape (Novljan, 2021). The circularity index was calculated using the formula:

$$C = \frac{4\pi S}{P^2}$$

where C is the circularity index, S is the surface area, and P is the perimeter length. Values between 0.9 and 1.0 indicate a circular shape, values between 0.8 and 0.9 an oval shape, and values below 0.8 an elongated or irregular shape (Suharyanto et al., 2020). The diameter was calculated by generating a rectangle by width for each daya, where the length of the longer side of the rectangle represents the maximum dimension along the principal axis of a daya. Orientation was derived using the convex hull geometry type, which calculates polygon orientation in degrees measured clockwise. Orientation patterns for each area are presented using rose diagrams. Depth was calculated as the difference between the highest point along the rim and the lowest point within the depression.

Table 1
Prevalent geomorphological setting for each study area.

Area 1, 2, 8	Planar surface
Area 3, 4	Palaeochannels
Area 5, 6, 7, 9, 10	Ridge and swale topography
Area 11	Combination of all three types

3.3. Sedimentological analysis

Sediment analyses were undertaken on samples collected from three dayas across the Nullarbor Plain. In total, five bulk sediment samples were obtained from depths between 10 and 20 cm, targeting relatively undisturbed sediment below the immediate surface layer. Three samples (see Fig. 2) were taken from the lowest point within individual dayas (samples 1, 3, 4), one from an elevated central position (sample 2), and one from the margin (sample 5). Despite the sparse sampling, the focus was on the central parts of the plain, where edge effects are minimal, primarily to characterise the basic sediment properties of the depressions, in a region where no systematic sediment sampling has been conducted. This represents an initial, reconnaissance-level dataset. The very shallow sediment infill, underlain by nodular calcrete and bedrock, also limits further excavation and sampling depth. Sample preparation, grain-size analysis and X-ray diffraction (XRD) analysis were carried out in the Physical Geography Laboratory of the Anton Melik Geographical Institute (ZRC SAZU) and in the laboratory of the Faculty of Natural Sciences and Engineering, University of Ljubljana.

Grain-size analysis was performed using a Malvern Mastersizer 3000 laser diffraction particle-size analyser. Representative subsamples were obtained by quartering and then transferred into vials. Deionised water and two drops of a 1% polysorbate-20 (Tween) surfactant solution were added to stabilise the suspension and prevent particle flocculation. The samples were sonicated for 10 s to disperse any remaining clay aggregates. For consistency and representativeness, only measurements with obscuration values between 15 and 25% were retained. Statistical processing of grain-size data was performed with the software Gradistat 9.1.

X-ray diffraction (XRD) analysis was undertaken using a Malvern Panalytical Empyrean III MultiCore powder diffractometer. Samples were pressed into pellets using a dedicated powder-sample holder with a 16-mm circular opening and loaded into an automated sample magazine. Measurements were collected from 3° to 70° 2θ, at a step size of 0.004° 2θ and a counting time of 12 s per step. Diffractograms were processed with HighScore+5.3a and the ICDD PDF-4/Minerals 2025 database. Qualitative and quantitative identification of mineral phases followed Rietveld refinement applied to the raw diffraction data.

3.4. Recent hydrological function

The recent hydrological function of dayas was assessed using the Modified Normalised Difference Water Index (MNDWI), derived from satellite remote sensing with Climate Engine tools (Climate Engine, 2024). The index is calculated from reflectance in the green band of the visible spectrum and short-wave infrared (SWIR) wavelengths. MNDWI enhances the detection of surface water and inundated areas and provides better differentiation from vegetation and built-up surfaces than the Normalised Difference Water Index (NDWI), which uses near-infrared (NIR) wavelengths (Moussaoui et al., 2024; Oštir, 2006; Xu, 2006). Based on an inspection of remotely sensed water surfaces following the floods that occurred in the western Nullarbor Plain in March 2024, a 300 km^2 area of inundated dayas near Rawlinna was selected for analysis. Water remained in these depressions for several months, from March through July. Monthly layers were obtained using the Climate Engine analytical tool from Sentinel-2 satellite imagery (Max Statistic, 10 m resolution). The raster layers were reclassified in ArcGIS Pro: values greater than 0 were assigned a value of 1, indicating open water, and values equal to or less than 0 were assigned NoData, indicating dry surfaces (Xu, 2006).

To estimate potential water loss through evaporation and infiltration, water surface area, volume, and the theoretical volume of evaporated water were calculated based on monthly average evaporation data (see Supplementary). Three dayas of comparable size, each retaining water for different durations, were selected. The volume of each daya was calculated from a DSM clipped to the polygons of inundated surfaces for each month of water presence. This was performed in QGIS using the

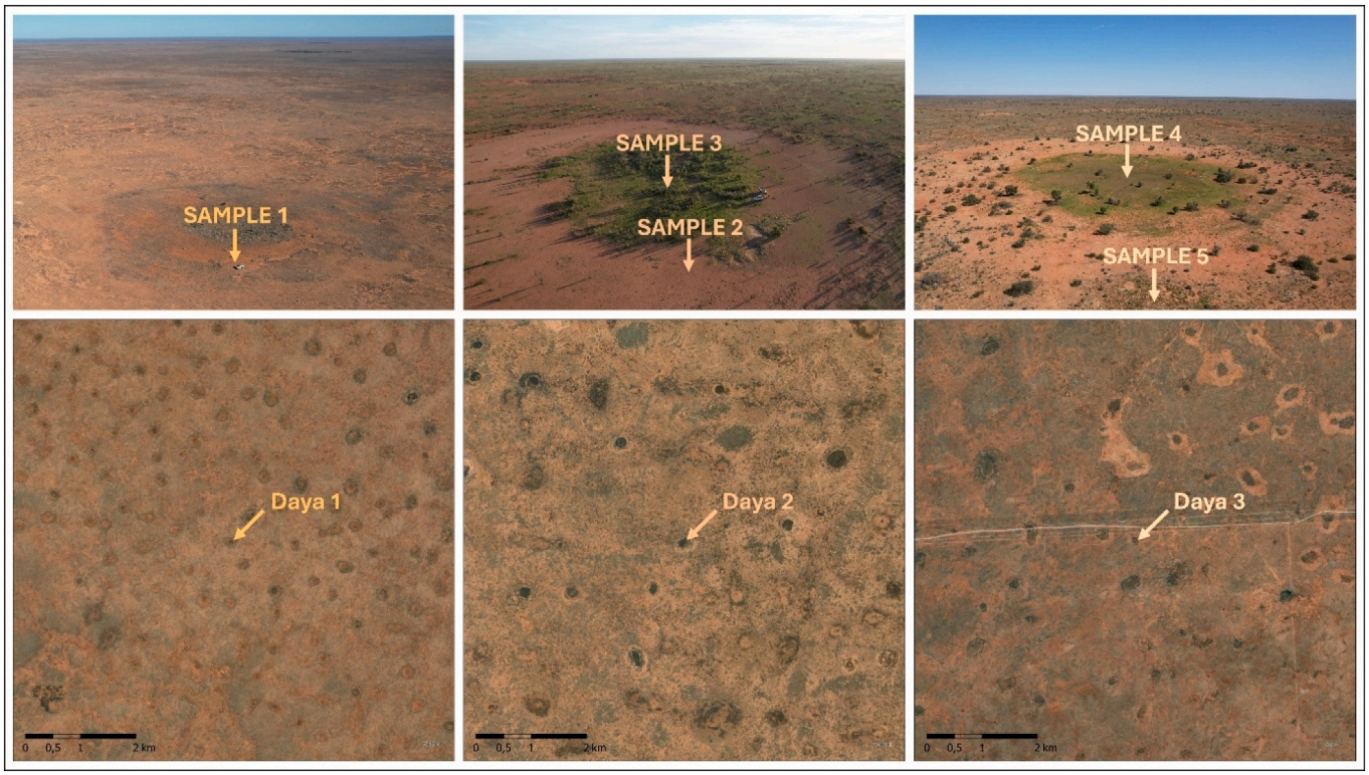

Fig. 2. Dayas with sampling sites and satellite imagery of the surrounding area. Locations correspond to Figs. 4 and 5, shown in Fig. 1. Basemap source: ESRI, 2025.

Raster Surface Volume tool, with the maximum elevation corresponding to the water-surface level from which volume was measured downward. Volumes were then subtracted to determine changes in water balance through time. Monthly averages were derived from long-term records (1975–2005) obtained using Class A evaporation pans and interpolation from a network of measurement stations across Australia (for details on the data measurement methodology see Bureau of Meteorology, 2006). Theoretical evaporation between satellite acquisitions was then estimated by converting monthly averages to daily values (monthly value divided by number of days), which were multiplied by the number of days between image dates within each month. Evaporation rates vary seasonally due to changes in climatic factors including air temperature, wind speed, and cloud cover, which control the energy available for evaporation (Brooks et al., 2013). The change in water volume due to theoretical evaporation was computed using:

$$\Delta V = E \times S \times \Delta t$$

where ΔV is the change in volume, E is the evaporation rate, S is the surface area and Δt is the time interval. The theoretical evaporative losses were then compared with the observed differences in calculated water volumes using GIS methods.

4. Results

4.1. Morphometric results and distribution

Remote sensing of closed depressions yielded 159,710 identified landforms throughout the Nullarbor Plain, with their morphometric characteristics presented in Table 2. Their mean surface area is 109,528m^2, mean diameter 452 m, mean circularity index 0.65 and mean depth 0.6 m. Within the detailed research areas (i.e., Areas 1–11), we identified a total of 7070 closed depressions with a mean surface area 86,490 m^2, a mean diameter 342 m, a mean circularity index 0.86 and a mean depth 1.4 m. These characteristics vary throughout the areas; for example, the mean surface area ranges from 31,316 m^2 to 268,519 m^2 (see Table 2 for the complete data). Percentages of dayas in study areas according to the circularity index and surface area are presented in Table 3 and Figs. 4 and 5, while orientation patterns for each area are presented using rose diagrams in Fig. 6.

Kernel density maps of dayas classified by size (see Fig. 3) reveal spatial patterns across the Nullarbor Plain. Small- and medium-sized dayas are predominantly concentrated in the south-western region and following the inland boundary of the Nullarbor Plain towards the north-eastern region. Large dayas (100,000–500,000 m^2) show the most even spatial distribution. The highest and most spatially extensive concentrations of the largest dayas occur in the southern Nullarbor Plain.

4.2. Sediment characteristics

Samples 2, 3, 4 and 5 are classified as sandy silt, whereas sample 1 corresponds to silty sand (see Fig. 7). Clay content is low across all samples, with the highest proportion in sample 2 (10.6%). Samples 1 and 4 are well sorted. Sample 2 is characterised by a relatively even distribution of silt and fine sand, while samples 1, 3 and 5 contain a higher proportion of coarse sand particles.

The dominant minerals are illite, quartz and kaolinite, while albite and calcite appear in smaller amounts, and anatase and hematite occur only in trace amounts. Sample 5 has the highest quartz content (49.4%), and sample 3 the lowest (19.1%). Samples 1–4 are relatively homogeneous regarding clay minerals: illite ranges between 36.7 and 40.1%, and kaolinite between 20.9 and 25.9%. Albite content is highest in sample 3 (12.9%) and lowest in sample 5 (1.4%). Calcite is more abundant in samples 2, 3 and 5, while it was not detected in sample 1. A marked difference in calcite content is also evident between samples 4 and 5 (0.6% and 8.2%). The complete X-ray diffraction results are presented in Table 4.

Table 2
Morphometric characteristics of closed depressions. For the location of study areas see Fig. 1.

Study area	Count	Density (daya/km^2)	Mean surface area (m^2)	Min surface area (m^2)	Max surface area (m^2)	Daya area (% of total study area)	Mean diameter (m)	Min diameter (m)	Max diameter (m)	Mean circularity	Min circularity	Max circularity	Mean depth (m)	Min depth (m)	Max depth (m)
1	323	1.1	98,232	3551	343,455	10.6	378	75	915	0.89	0.63	0.98	1.9	0.2	5.2
2	1397	4.7	39,733	1284	195,913	18.5	228	44	657	0.91	0.53	1.00	1.4	0	3.3
3	1077	3.6	40,025	1009	339,195	14.4	261	46	1120	0.83	0.27	0.99	2.0	0	6.2
4	1373	4.6	31,316	1183	244,781	14.4	212	45	935	0.87	0.37	0.98	1.2	0	3.4
5	273	0.9	219,432	3122	1,535,880	20.0	644	76	3056	0.78	0.31	0.95	1.7	0.1	4.7
6	440	1.5	165,505	1309	1,232,890	24.3	521	46	1796	0.77	0.32	0.98	1.4	0	4.2
7	376	1.3	268,519	2363	2,287,240	33.7	661	53	3206	0.80	0.31	0.96	1.4	0.1	3.2
8	378	1.3	220,069	10,102	2,089,471	27.7	585	117	3067	0.86	0.38	0.96	1.0	0.2	2.1
9	567	1.9	69,182	4760	284,592	13.1	375	93	1094	0.82	0.47	0.98	3.0	0.4	6.1
10	214	0.7	156,957	13,572	786,753	11.1	491	139	1455	0.90	0.52	0.98	0.6	0	1.6
11	652	2.2	74,585	4492	522,720	16.1	336	77	1548	0.89	0.28	0.98	1.0	0	2.9
Mean all areas	643	2.1	86,490	4250	895,626	18.5	342	74	1714	0.86	0.40	0.98	1.4	0.1	3.9
Entire research area	159,710	0.9	109,528	431	4,272,111	10.1	452	25	5058	0.65	0.10	1.00	0.6	0	11.9

4.3. Hydrological functioning of dayas

In March 2024, tropical moist air masses approached the western Nullarbor Plain from the northwest. The resulting heavy rainfall triggered flash flooding (see Fig. 8). Weather stations across the Eucla region recorded the highest March rainfall since the beginning of measurement: Eucla on the southern coast received 40.4 mm, Forrest in the central part 58.0 mm, while Bull Camel and Seemore Downs near Rawlinna in the western part received 268.4 and 333.4 mm, respectively (Bureau of Meteorology, 2024b). Water accumulated in topographic depressions, where it remained for several months according to Sentinel-2 imagery (Climate Engine, 2024).

Fig. 9 shows Area 12 southeast of Rawlinna (see Fig. 1), where water persisted in dayas from March through July. Larger water bodies formed in the southern and eastern parts of the area, where topography is lower. In several instances, the water surface extended across neighbouring dayas, merging them into a single water-filled depression. Three dayas of broadly comparable size (marked by arrows in Fig. 9) that retained water for differing durations were further analysed (for detailed calculations and visualisations see Supplementary). Daya 2 dried the most rapidly; it is situated in a locally lower section of the southeastern area. Daya 1 (see Fig. 10), positioned on a relatively higher central section, dried next. The longest-lasting water body was in daya 3, which lies on a relatively elevated part of the southwestern area.

5. Discussion

The final dataset contains 159,710 mapped closed depressions and represents the most comprehensive and systematic mapping of these features to date. It provides a robust, spatially consistent foundation for subsequent analyses of closed-depression distribution and morphology.

As with any automated landform recognition approach (e.g., Shirani et al., 2023; Stefanovski et al., 2024; van der Meij et al., 2021), it would be unrealistic to expect the complete identification of every individual daya across the Nullarbor Plain. This limitation is particularly relevant in areas of very subdued relief, locally variable digital elevation model quality, or where closed depressions occur that may not represent dayas sensu stricto.

The present dataset is the result of the recognition of closed depressions based on the TanDEM-X digital elevation model, which proved most suitable for the Nullarbor Plain at the regional scale. The incorporation of radiometric imagery and manual identification of closed depressions within selected detailed study areas significantly improved feature recognition and informed subsequent analyses of Nullarbor Plain dayas. Nevertheless, the full shapefile of closed depressions should be interpreted with appropriate caution. Radiometric data were not used for automated recognition because potassium, thorium and uranium radiometric signatures of sediment layers vary across the Nullarbor Plain, making automated classification prone to erroneous results.

There is no formal criterion defining the minimum size at which an inception depression becomes a daya, a challenge which is a part of hierarchical issues in theoretical geomorphology (Evans, 2012; Smith and Mark, 2003). Similarly, there is no fixed upper size limit for dayas. In this study, coalescent dayas with connected floors were mapped as single forms and were not excluded, as their removal would artificially imply an absence of depressions in areas where they clearly exist as merged features. For analytical consistency, features with diameters smaller than 25 m and larger than 5 km were excluded from further analysis.

Because the morphometric approach does not distinguish between genetic types, features of different origin may be grouped together. However, the applied minimum and maximum diameter thresholds automatically exclude smaller features such as blowholes, as well as very large-scale depressions. Other types of closed depressions do occur on the Nullarbor Plain, including some collapse dolines that may be surrounded by shallow sedimentary aprons formed by localised sediment

Table 3
Percentages of dayas in study areas according to the circularity index and surface area.

		Small (≤50,000 m^2)	Medium (50,000–100,000 m^2)	Large (100,000–500,000 m^2)	Largest (>500,000 m^2)	Total
Area 1	Elongate or irregular (≤0.80)	4.0	1.5	5.0	0	10.5
	Oval (0.81–0.91)	10.2	8.4	16.7	0	35.3
	Circular (0.91–1.00)	15.5	15.2	23.5	0	54.2
	Total	29.7	25.1	45.2	0	100
Area 2	Elongate or irregular (≤0.80)	3.8	1.4	0.6	0	5.9
	Oval (0.81–0.91)	13.1	2.3	0.9	0	16.3
	Circular (0.91–1.00)	55.4	16.5	5.9	0	77.8
	Total	72.3	20.3	7.4	0	100
Area 3	Elongate or irregular (≤0.80)	13.9	9.1	6.3	0	29.3
	Oval (0.81–0.91)	29.6	5.6	1.4	0	36.6
	Circular (0.91–1.00)	29.4	3.4	1.2	0	34.1
	Total	73.0	18.1	8.9	0	100
Area 4	Elongate or irregular (≤0.80)	9.5	4.3	2.0	0	15.9
	Oval (0.81–0.91)	32.3	3.3	1.6	0	37.2
	Circular (0.91–1.00)	38.8	6.0	2.1	0	46.9
	Total	80.6	13.6	5.8	0	100
Area 5	Elongate or irregular (≤0.80)	6.2	4.8	26.0	7.7	44.7
	Oval (0.81–0.91)	11.7	7.0	20.1	1.1	39.9
	Circular (0.91–1.00)	5.9	4.8	4.4	0.4	15.4
	Total	23.8	16.5	50.5	9.2	100
Area 6	Elongate or irregular (≤0.80)	12.7	7.3	22.3	6.1	48.4
	Oval (0.81–0.91)	19.3	5.5	12.0	0.5	37.3
	Circular (0.91–1.00)	9.8	1.4	3.2	0	14.3
	Total	41.8	14.1	37.5	6.6	100
Area 7	Elongate or irregular (≤0.80)	6.6	6.1	15.7	11.4	39.9
	Oval (0.81–0.91)	7.7	6.6	21.3	1.3	37.0
	Circular (0.91–1.00)	4.0	5.1	13.6	0.5	23.1
	Total	18.4	17.8	50.5	13.3	100
Area 8	Elongate or irregular (≤0.80)	0.3	0.3	9.3	8.7	18.5
	Oval (0.81–0.91)	1.1	5.3	20.9	1.6	28.8
	Circular (0.91–1.00)	6.3	16.9	29.4	0	52.6
	Total	7.7	22.5	59.5	10.3	100
Area 9	Elongate or irregular (≤0.80)	11.6	13.6	10.4	0	35.6
	Oval (0.81–0.91)	17.5	18.5	7.4	0	43.4
	Circular (0.91–1.00)	9.3	9.0	2.6	0	21.0
	Total	38.4	41.1	20.5	0	100
Area 10	Elongate or irregular (≤0.80)	0.5	0.5	8.4	0.5	9.8
	Oval (0.81–0.91)	3.7	10.3	13.1	0.5	27.6
	Circular (0.91–1.00)	7.0	20.6	34.6	0.5	62.6
	Total	11.2	31.3	56.1	1.4	100
Area 11	Elongate or irregular (≤0.80)	3.4	1.7	4.9	0.2	10.1
	Oval (0.81–0.91)	15.8	8.4	8.1	0	32.4
	Circular (0.91–1.00)	23.5	20.7	13.3	0	57.5
	Total	42.6	30.8	26.4	0.2	100

transport. These, however, represent a negligible component of the overall dataset. Slightly more than 300 collapse dolines have been documented, compared with more than 150,000 dayas identified in this study. While this affects the full closed depression shapefile, it does not compromise the clarity of interpretations based on the selected and manually refined study areas. For this reason, the study adopted both a wide-scope mapping approach and a narrow-scope, detail-focused analytical strategy.

5.1. Morphological and morphometric characteristics

The 11 detailed study areas (see Figs. 4 and 5) show that the spatial distribution and morphometric characteristics of dayas on the Nullarbor Plain are not even, but closely correspond to inherited palaeotopography. Three major geomorphological settings are presented in the following paragraphs: planar surfaces, palaeochannel-dominated area, and ridge–swale topography systems.

Areas 1, 2 and 8 are located on planar surfaces, characterised by flatness and negligible relief. Dayas in these areas have high circularity indices (mean 0.86–0.91) and moderate mean diameters (228–585 m) (see Table 2). In Area 2, for example, circular forms constitute 77.8% of mapped depressions (see Table 3), whereas elongate or irregular forms remain in minority. Densities vary considerably, reaching 4.7 dayas/km^2 in Area 2 but only 1.1 dayas/km^2 in Area 1, but this is correlated to the mean surface area of dayas, where larger dayas generally represent a lesser number per km^2. Daya alignments from rose diagrams (see Fig. 6) show relatively negligible patterns, however, Area 2 shows minor NW-SW and SW-NE alignment pattern, and Area 8 shows minor NW-SW alignment pattern. Whilst the alignment pattern in Area 2 cannot be clearly explained by surrounding topography and may therefore indicate the structural control (e. g. joints, fractures), the alignment in Area 8 is comparable to ridge and swale topography alignment, which becomes apparent ~15 km NW from the area, but is not identifiable within the detail area itself. This suggests that the alignments of dayas on planar surfaces, which are not structurally controlled, may reflect an ancient topography, which has been subsequently eroded.

Areas 3 and 4 are dominated by fluvial palaeochannels (Alley et al., 1999; Lowry and Jennings, 1974). Here, mean diameters are smaller (212–261 m), and circularity indices are slightly lower (0.83–0.87) compared to dayas on planar surfaces. Elongate or irregular forms constitute 29.3% of depressions in Area 3 and 15.9% in Area 4. These areas exhibit relatively high densities (3.6–4.6 dayas/km^2), reflecting numerous small depressions associated with drainage-controlled environments. Daya alignments from rose diagrams (see Fig. 6) show relatively negligible patterns, however, they are more random where the palaeochannels have a dominant dendritic type (Area 3) compared to where palaeochannels are in places rectangular due to joint/fault control (Area 4).

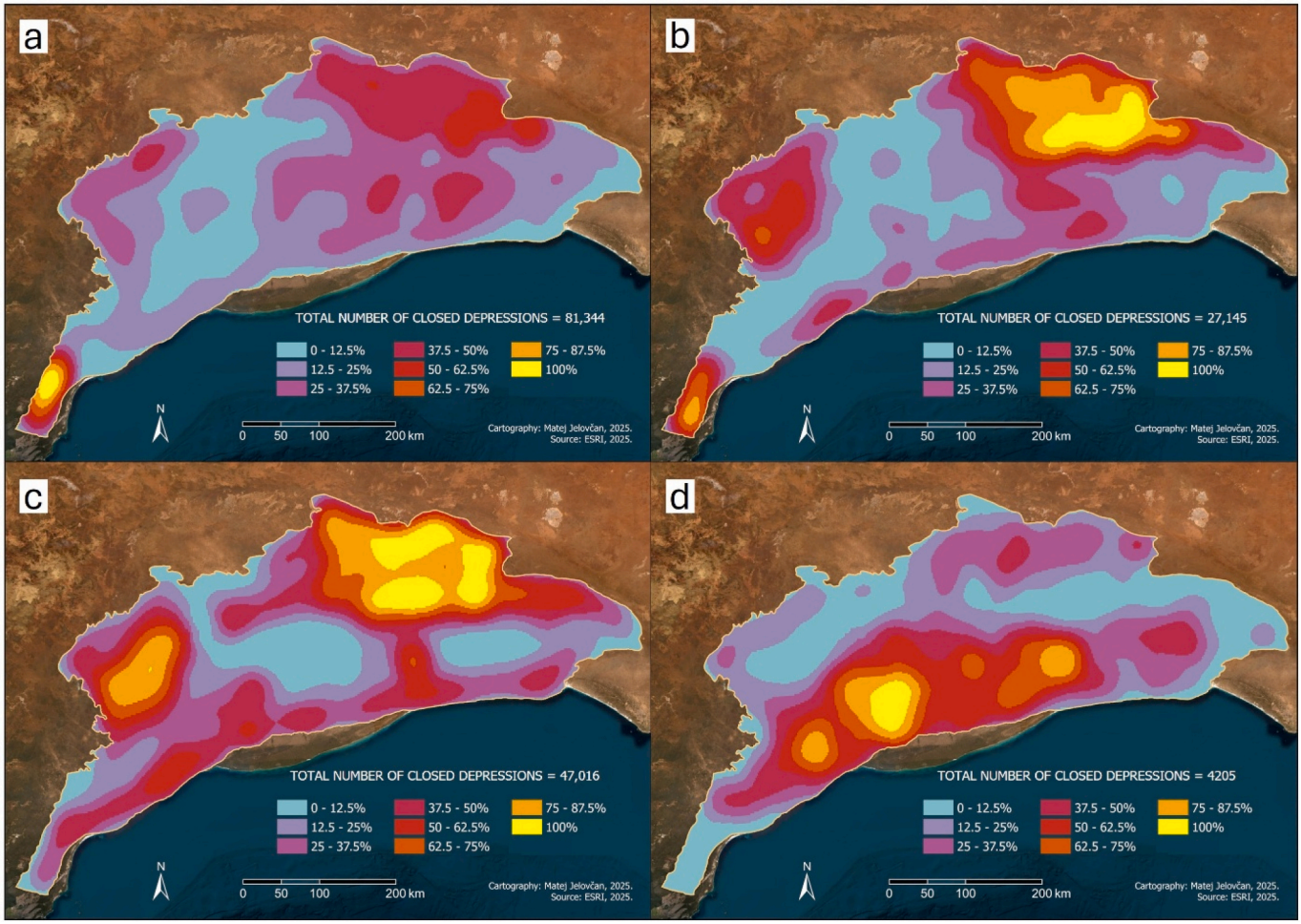

Fig. 3. Kernel density maps for each surface area class in %; a) small, b) medium-sized, c) large and d) largest. Basemap source: ESRI, 2025.

Table 4
X-ray diffraction results (%). For sample locations see Figs. 1 and 2.

Mineral	Sample 1	Sample 2	Sample 3	Sample 4	Sample 5
Illite	39.7	37.0	36.7	40.1	26.4
Quartz	31.5	25.4	19.1	25.4	49.4
Kaolinite	21.8	23.1	20.9	25.9	14.2
Albite	6.3	7.5	12.9	7.3	1.4
Calcite	0	6.6	9.6	0.6	8.2
Anatase	0.4	0.5	0.6	0.5	0.2
Hematite	0.3	0	0.1	0.2	0.2

Areas 5, 6, 7, 9 and 10 represent the ridge–swale terrain. In general, ridge-swale terrain is genetically derived from superimposed longitudinal dune systems, now imprinted into the Nullarbor Limestone (Burnett et al., 2020). However, in places, ridge-swale terrain may also reflect tectonic/structural lineaments (Clark, 2012; Krapf and González-Álvarez, 2018; Sellmann et al., 2022). In both cases, dayas are affected by similar topography and are thus joined together. These areas contain the largest mean diameters (up to 661 m) and the highest proportions of large and very large dayas (up to 63.8%). Elongate or irregular forms dominate (39.9–48.4%), while circular forms are comparatively less frequent (14.3–23.1%). Maximum diameters exceed 3 km in Areas 5 and 7. Densities are lower (0.9–1.5 dayas/km^2) than in palaeochannel-dominated regions, reflecting the predominance of large coalesced depressions within swales. Alignment patterns from rose diagrams (see Fig. 6) closely match ridge direction trends, confirming directional topographic control. This suggests that the morphology and morphometry are strongly controlled by either inherited dune geometry or structural lineaments, where swales concentrate runoff and accumulate thicker, less permeable sediment infill, promoting prolonged ponding (Gillieson et al., 1994) and lateral coalescence of depressions. In contrast, ridge crests favour infiltration (Gillieson et al., 1994) and support smaller, isolated circular forms on top of the crests. Smaller dayas are usually associated with higher topographic position (on crests) and consequently limited dissolution dynamics.

Area 11 is an example of a combination of ridge-swale terrain, palaeochannels and flat individual areas. In this case, the mean diameter of dayas reflects a moderate size, and includes all types of dayas, although circular type prevails.

Across all study areas, mean depths remain uniformly low (0.6–3.0 m), despite large differences in surface area and diameter. This suggests that morphometric variability is primarily expressed in planform size and geometry rather than vertical incision. On the other hand, circular dayas in general tend to be smaller on the eastern part of the Nullarbor Plain. This pattern coincides with allochthonous sediment input from palaeodrainage systems (see Fig. 1) forming a large alluvial fan sourced in adjacent uplands (Alley et al., 1999), which may promote more diffuse infiltration (Al-Halbouni et al., 2021; Salomon and Pulina, 2005; Veress and Méhes, 2021). In contrast, the western part of the study area is occupied by an extensive depression that was excluded from the analysis. Lower rainfall in the eastern part of the plain (see Fig. 1, Bureau of Meteorology, 2024a) may further limit enlargement.

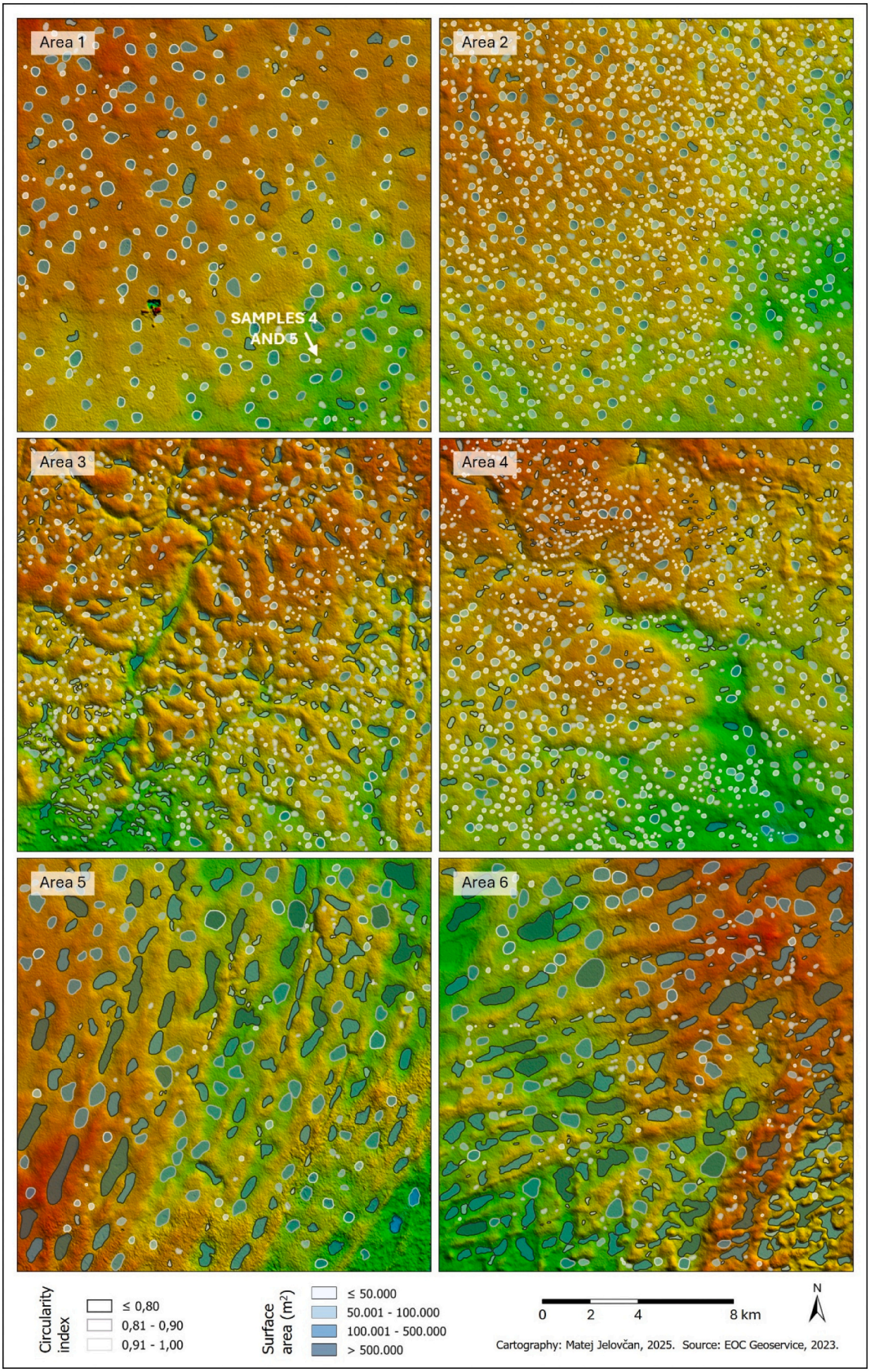

Fig. 4. Circularity index and surface area for dayas in study areas 1–6, arrow shows sampled daya. Basemap source: EOC Geoservice, 2023.

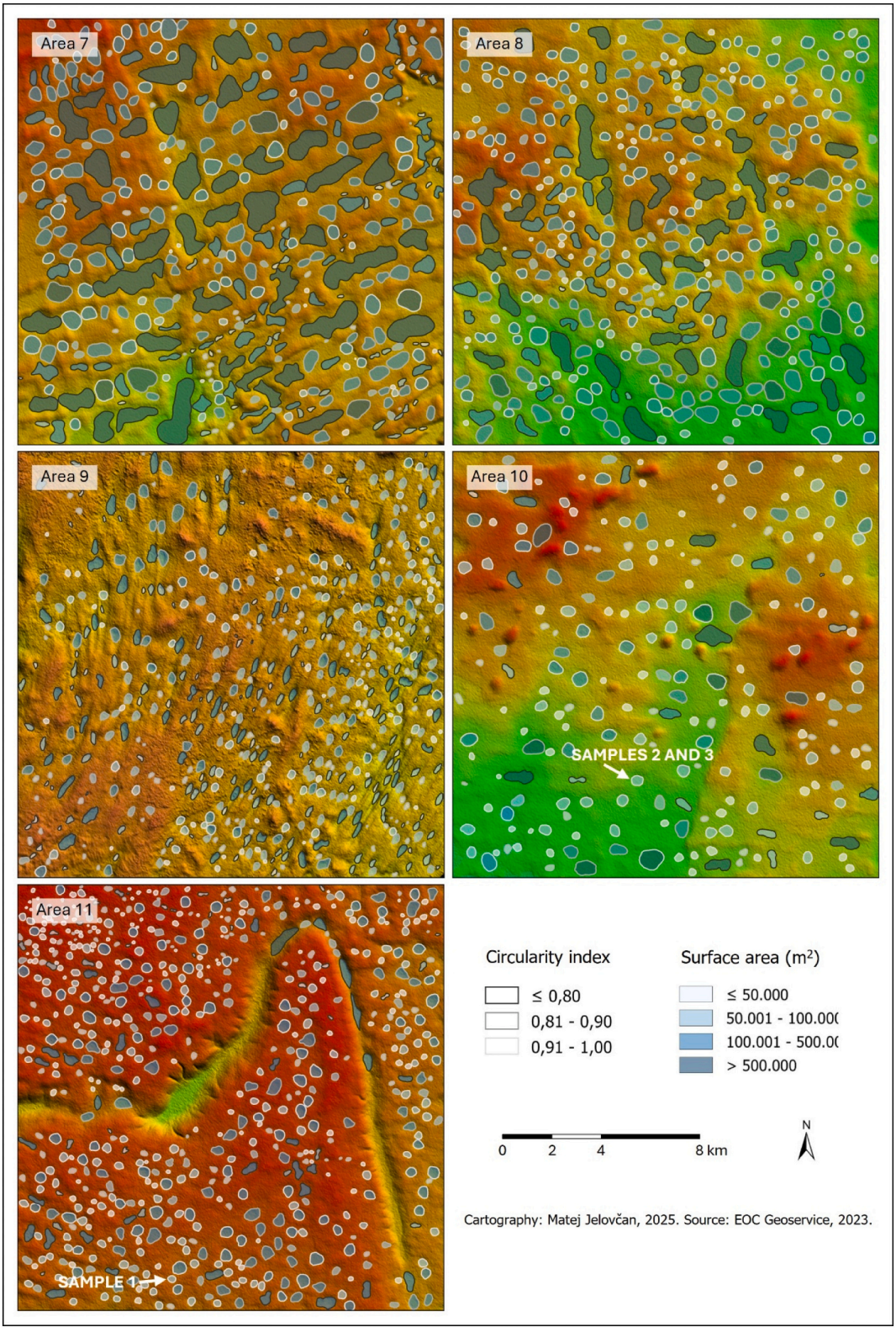

Fig. 5. Circularity index and surface area for dayas in areas 7–11, arrows show sampled dayas. Basemap source: EOC Geoservice, 2023.

5.2. Relation to Goudie's daya typology

Goudie (2010) distinguishes several daya types based on morphological and morphogenetic traits, including the simple circular type, drainage channel type, centripetal type, structurally controlled type and wind-aligned type. Within the present dataset, only the circular type can be directly and objectively supported by morphometric parameters, as high circularity indices (≥0.90) correspond to planforms approaching circular geometry (Suharyanto et al., 2020).

In planar settings, the dominance of circular and oval depressions with high circularity indices indicates widespread occurrence of Goudie's circular type (Goudie, 2010). These depressions typically occur as

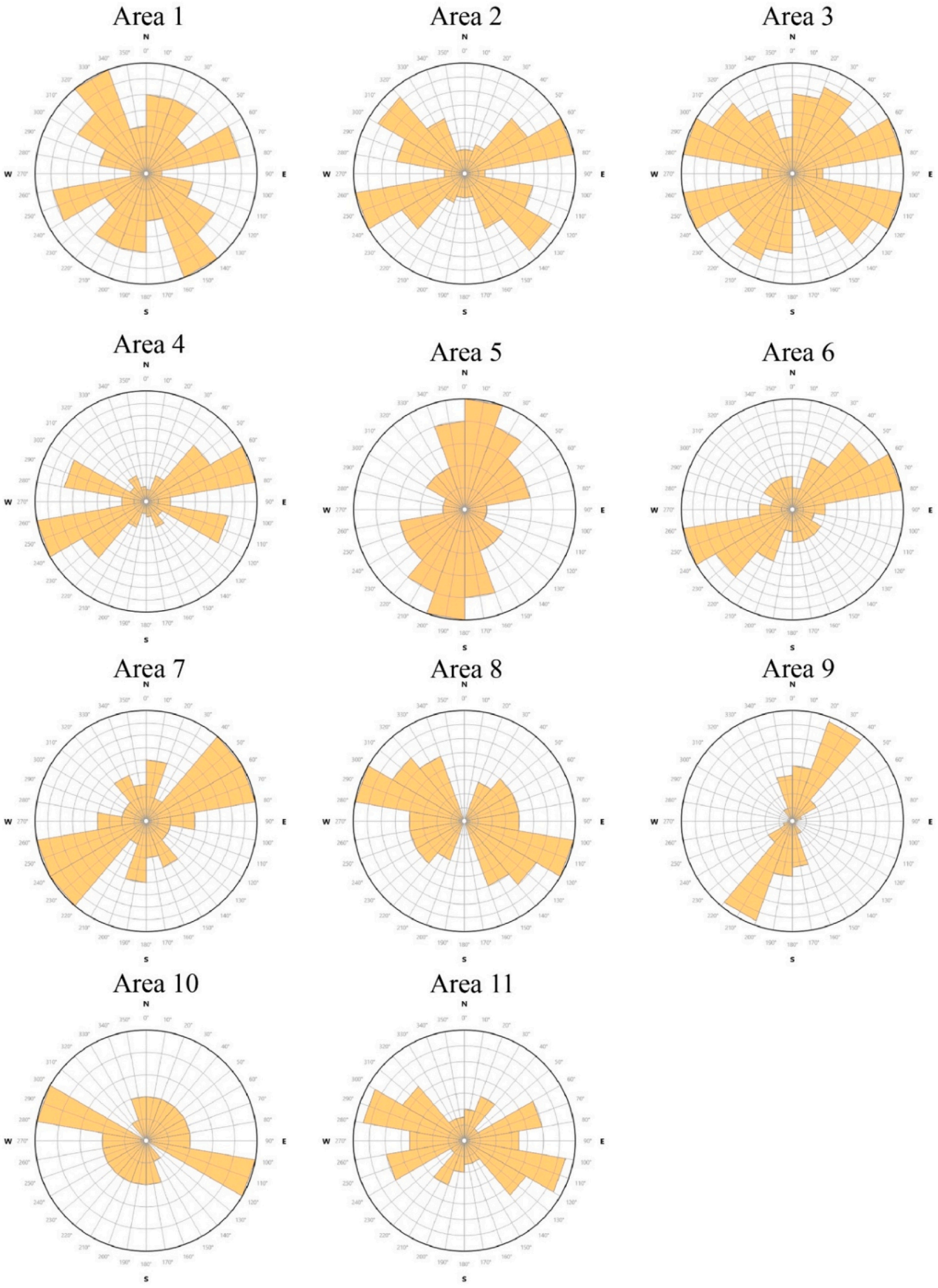

Fig. 6. Rose diagrams for each study area.

isolated forms on subdued palaeotopography (see Figs. 4 and 5). In palaeochannel-dominated areas, elongate and irregular depressions frequently coincide with mapped shallow drainage networks (Alley et al., 1999). While circularity alone does not determine genetic type, their spatial association with palaeochannels supports interpretation as drainage channel types sensu Goudie (2010). Where multiple shallow inflow channels converge into a single depression (see Fig. 11), the morphology corresponds to the centripetal type described by Goudie (2010). In ridge–swale dune systems, elongate and compound depressions aligned with former dune axes correspond to the wind-aligned type (Burnett et al., 2020; Goudie, 2010). In these areas, moderately negative correlations between size and circularity indicate that larger depressions tend to be more elongate, reflecting confinement and coalescence within swales rather than distinct morphogenetic processes. Wind-aligned dayas may have formed either during active dune development or later on stabilised palaeodune surfaces; however, as their alignment reflects inherited surface morphology rather than bedrock structure, they are not classified as structurally controlled types. The recognised daya types are shown in Fig. 11.

The structurally controlled type cannot be reliably distinguished from morphometric parameters (e.g., length) alone, but local linear alignments clearly coincide with known faults or fault-guided palaeochannels (e.g., individual examples in Area 11 were detected in fault-guided fluvial palaeochannel).

5.3. Sediment infill and recent hydrological activity

Sedimentological and hydrological evidence indicates that dayas on the Nullarbor Plain are not relict features but are actively modified through episodic flooding and sediment redistribution. XRD analysis (see Table 4) reveals dominant siliciclastic components (89.6–99.3%), with little to no authigenic carbonate (0–9.6%), derived from weathering.

Texturally, sediments are characterised as sandy silt and silty sand (see Fig. 7), and are generally well sorted reflecting aeolian and fluvial influences. The provenance is largely the non-carbonate hinterland, e.g. the Great Victoria Desert (see Fig. 1). The coarse sand fraction is minor (1.0–5.5%), due to its limited aeolian mobility.

The central parts of dayas remain flooded for longer periods, enhancing the trapping and stabilization of fine-grained aeolian sediments. Shallow channels incising from daya margins towards centres and the presence of weathered calcrete fragments observed during fieldwork, are consistent with observations from North African dayas (Clarke et al., 1974; Mitchell and Willimott, 1974), and reflect episodic runoff, flood sediment deposition and/or vertical sediment movement following wet-dry cycles. In addition, higher vegetation density reduces deflation of mobile silt and fine sand and enhances the trapping of entrained aeolian sediment, leading to the formation of mound like depositional features (Clarke et al., 1974; Gillieson et al., 1994; Goudie, 2004). Compared with the surrounding planar surface (sample 5), daya floors show more effective sorting, greater clay accumulation, and reduced carbonate content, attributed to subsurface leaching and dissolution (Clarke et al., 1974; Mitchell and Willimott, 1974), while daya slopes commonly contain weathered calcrete fragments.

The predominantly siliciclastic content in daya sediments (quartz, illite, and kaolinite), together with a silty and clay rich texture, forms a semi-permeable hydrological barrier that can promote episodic water ponding lasting from several days (Gillieson et al., 1994) to months as observed from Sentinel satellite imagery (Climate Engine, 2024). However, water does not pond in all dayas, suggesting that in some cases sediment permeability is sufficiently high to allow concurrent infiltration into the subsurface. In addition, variability of inundation following the March 2024 flood event (see Fig. 9) indicates control by local topographic lows, depression depth, and sediment thickness and permeability. Across all analysed dayas (see Supplementary), calculated water losses consistently exceeded theoretical evaporation, providing evidence for active infiltration into the karst aquifer, in line with previous interpretations (Capot-Rey, 1939; Clarke et al., 1974; Gautier, 1951; Jennings, 1983; Mitchell, 1970; Mitchell and Willimott, 1974).

The absence of evaporite minerals (e.g., halite and gypsum in daya sediments) further supports drainage to subsurface rather than complete evaporation. Infiltration is likely enhanced by vegetation-induced macroporosity (Li et al., 2011). Fine-grained sediment facilitates capillary and lateral water movement (Veress, 2017), while elevated biogenic CO_2 and organic acids increase water acidity and promote limestone dissolution. Consequently, ponded water enlarges depressions laterally and vertically by dissolution, whereas ongoing sediment accumulation maintains shallow depth of dayas. This indicates that dayas on the Nullarbor Plain remain geomorphically active and continue to undergo dissolution-driven expansion despite arid climate conditions, which have prevailed on the Nullarbor Plain since the late Pliocene (Miller et al., 2012).

The March 2024 flood also allows the hydrological role of dayas to be expressed in terms of event-based recharge efficiency. Assuming that the

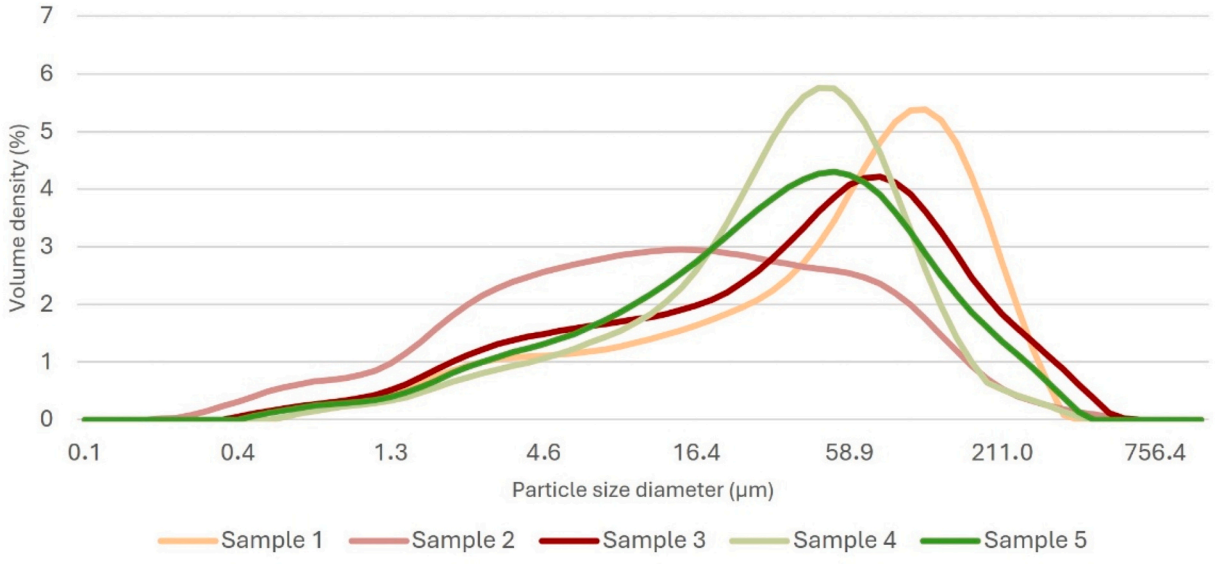

Fig. 7. Particle size distribution.

Fig. 8. Dayas with ephemeral lakes near Rawlinna. Trans-Australian Railway at the bottom of the image for the scale.

contributing catchment of Daya 1 was approximately three to five times the mapped daya area, and using the observed rainfall range of 268.4 and 333.4 mm across the western Nullarbor (Bureau of Meteorology, 2024b), the residual water loss after subtraction of theoretical evaporation indicates that approximately 25–30% of rainfall falling across the daya catchment may have infiltrated below the depression floor. Although this estimate is necessarily approximate because catchment area, water depth, and infiltration pathways are not directly measured, it shows that dayas can operate as highly efficient focused recharge features during extreme rainfall events. This interpretation contrasts with the generally low rates of long-term diffuse recharge expected across arid and semi-arid Australia, as demonstrated by Lee et al. (2024), and suggests that localised recharge through closed depressions, ephemeral ponds, karst conduits, and preferential-flow pathways may represent a disproportionately important component of the Nullarbor groundwater system. This high inferred recharge efficiency is also consistent with the general behaviour of dryland aquifers, which are not karstic but where recharge is also often episodic and threshold-controlled rather than continuous. For example, in central Australia, numerical modelling showed that only rainfall events exceeding approximately 150–200 mm produced noticeable groundwater recharge, with recharge linked to monsoonal extreme rainfall events (Boas and Mallants, 2022).

5.4. Chronological implications and broader significance

The formation of karst features in arid environments is commonly linked to past wetter climatic phases (Ford and Williams, 2007; Salomon and Pulina, 2005). On the Nullarbor Plain, the last warm and humid period occurred during the Pliocene (ca. 5–3 Ma) (Sniderman et al., 2016; Woodhead et al., 2019), when palaeochannels were active (Alley et al., 1999) and dune systems were superimposed onto the limestone bedrock (Burnett et al., 2020). Regional differences in daya characteristics demonstrate that their formation was spatially variable: in northern and eastern sectors, dayas likely developed following palaeochannel incision or dune removal, whereas in the southern Nullarbor Plain they may have formed contemporaneously with dune-system karstification or later. Dayas can therefore be regarded as Pliocene or younger features based on their strong dependence on preserved palaeotopography.

Preserved palaeotopography exerts a first-order control on the distribution, morphology, and evolution of dayas in arid karst landscapes. The strong correspondence between daya orientation, relict dune alignments, palaeochannel systems, and subdued topography underscores the importance of long-term landscape inheritance and demonstrates that daya development is primarily governed by inherited surface structure.

Beyond the Nullarbor Plain, the results provide broader implications for understanding closed-depression development on low-relief carbonate platforms in arid to semi-arid climates. The combined morphometric, sedimentological and hydrological evidence demonstrates that large populations of shallow depressions can remain geomorphically active under present-day aridity through the interaction of inherited palaeotopography, episodic flooding, fine-grained sediment accumulation, and focused dissolution. This challenges the common assumption that such depressions are predominantly relict features formed exclusively during past humid phases. Instead, the Nullarbor Plain dayas illustrate how subtle topographic inheritance can localise water, sustain dissolution, and maintain morphodynamic activity over multimillion-year timescales despite limited rainfall. The integration of regional-scale DEM analysis with targeted sedimentological and hydrological validation further demonstrates an effective methodological framework for analysing large closed-depression fields elsewhere. Similar approaches may therefore help to reassess the origin, longevity and activity of depressions on other planar carbonate terrains.

6. Conclusion

This study presents the most comprehensive mapping of shallow closed depressions (dayas) on the Nullarbor Plain to date, combining DEM analysis, radiometric imagery, and targeted manual identification. The dataset of over 150,000 features provides a robust foundation for understanding the distribution, morphology, and evolution of dayas at both regional and local scales. Morphometric analyses reveal that variation in size, shape, and alignment is strongly controlled by inherited palaeotopography, including planar surfaces, palaeochannel-dominated

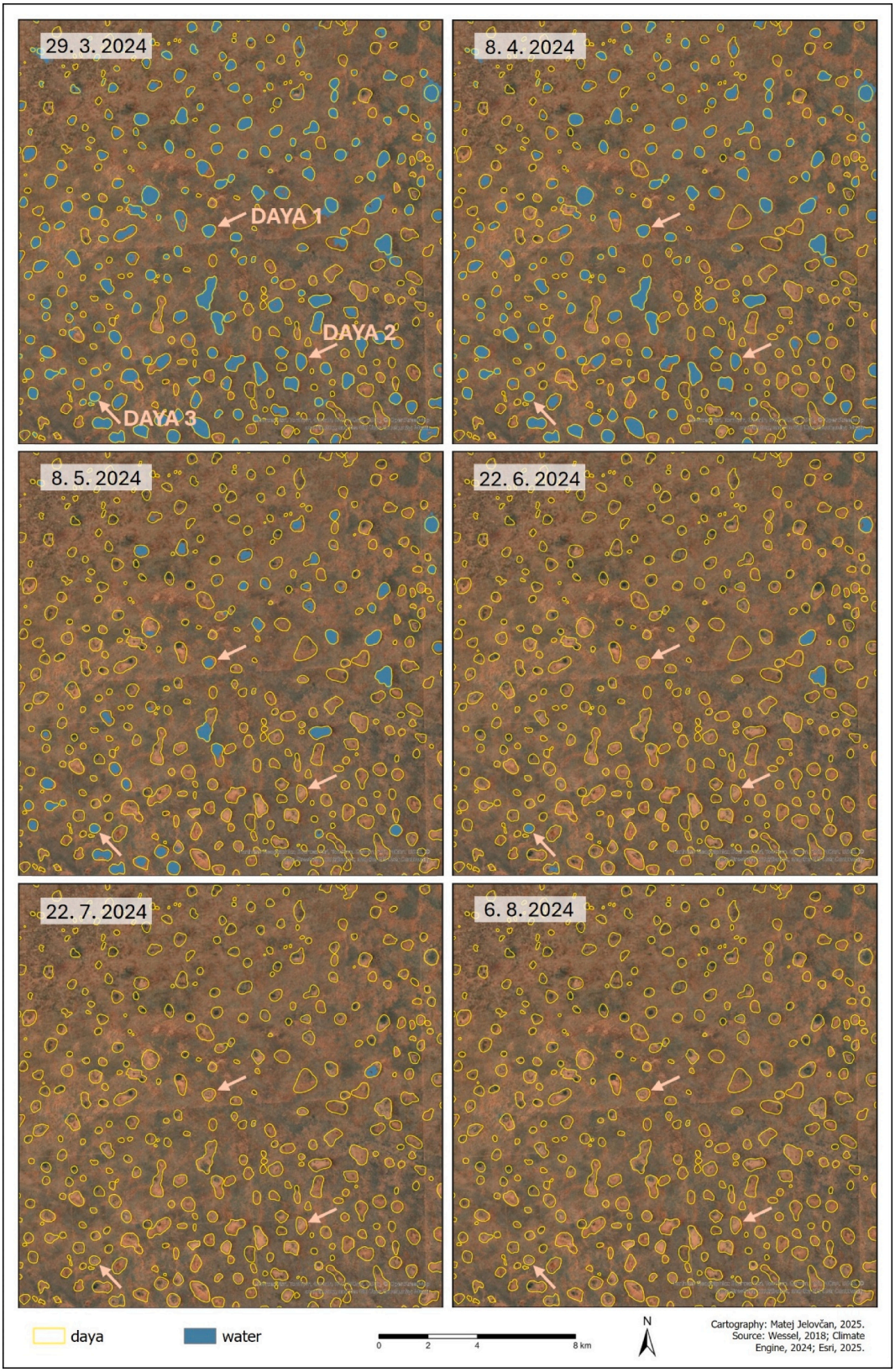

Fig. 9. Ephemeral lakes of the study area 12 (time span from March to August 2024). Location shown in Fig. 1. Basemap source: ESRI, 2025.

areas, and ridge–swale topography systems. Sedimentological and hydrological evidence confirms that dayas are geomorphically active, with episodic flooding, sediment redistribution, and limestone dissolution continuing to modify depressions under the present arid climate and potentially contributing to focused event-based groundwater recharge. Spatial differences in morphometry and sediment infill indicate that dayas reflect a combination of inherited landscapes and ongoing processes, challenging the notion that shallow depressions on arid

DAYA 1

March (29. 3. 2024)

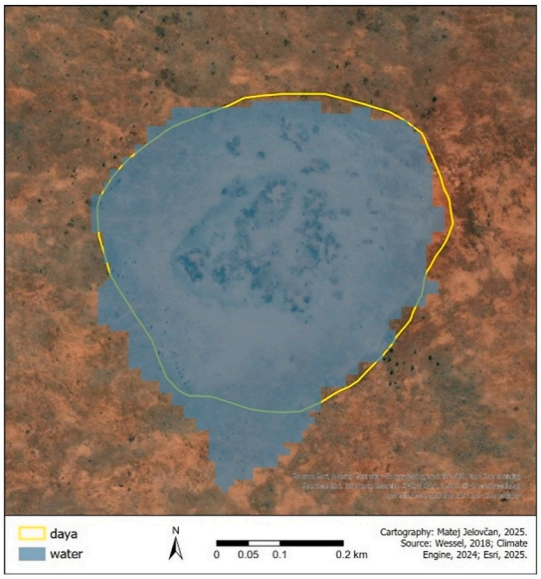

S = 228,243.0 m^2
V = 154,604.8 m^3

Mean E = 250–300 mm/month

April (8. 4. 2024)

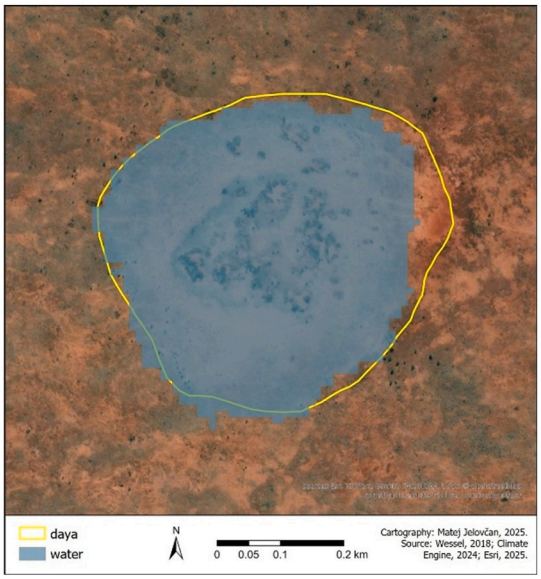

S = 196,837.0 m^2
V = 133,995.3 m^3
Change in volume: **20,609.5 m^3**
Mean E = 175–200 mm/month
→ in 10 days, the theoretical evaporation would range between 14,287.8 and 16,661.6 m^3

May (8. 5. 2024)

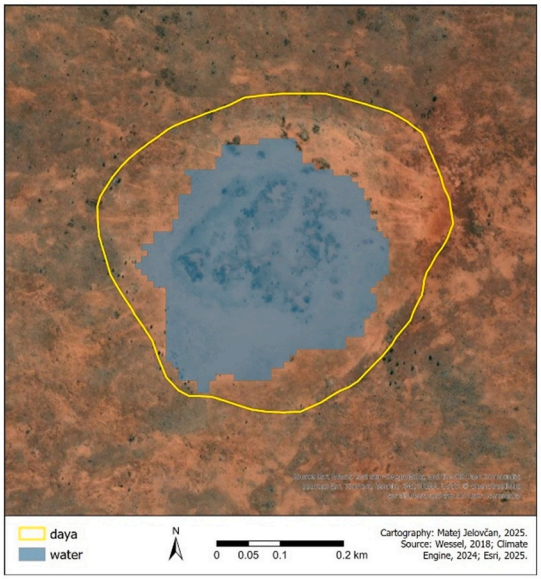

S = 106,533.0 m^2
V = 25,597.0 m^3
Change in volume: **108,398.3 m^3**
Mean E = 125–150 mm/month
→ in 30 the theoretical evaporation would range between 31,415.8 in 36,572.0 m^3

June (22. 6. 2024)

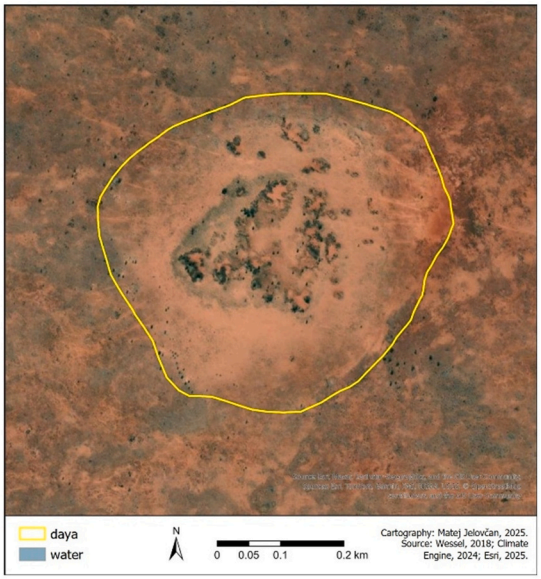

S = 0 m^2
V = 0 m^3
Change in volume: **25,597.0 m^3**
Mean E = 100–125 mm/month
→ in 45 the theoretical evaporation would range between 17,535.5 in 21,609.6 m^3

Fig. 10. Calculated change in the amount of water in daya 1 and theoretical evaporation. Basemap source: ESRI, 2025.

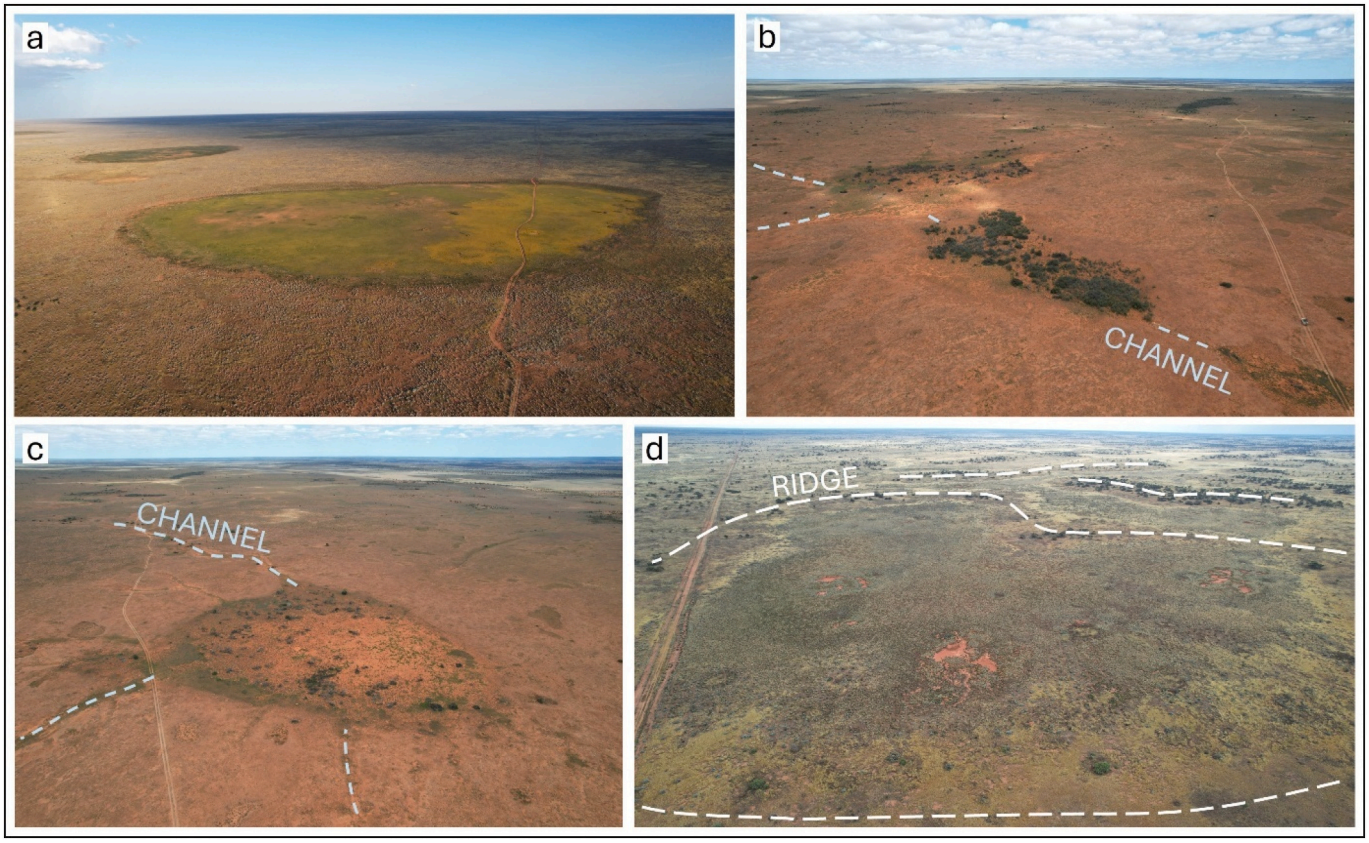

Fig. 11. Different daya types: a) large circular dayas in the west central Nullarbor Plain, b) elongate drainage channel type dayas interconnected with shallow channels in the northeast, c) a centripetal type daya with shallow inflow channels in the northeast, d) a wind aligned type daya situated in the swale of the relict limestone imprinted longitudinal dune system in the south (classification from Goudie, 2010). Dirt tracks for scale.

carbonate plains are predominantly relict. This provides a valuable insight into karst evolution on arid planar carbonate platforms worldwide, along with a transferable framework for their analysis.

CRediT authorship contribution statement

Matej Jelovčan: Writing – original draft, Visualization, Methodology, Investigation, Formal analysis, Data curation, Conceptualization. **Uroš Stepišnik:** Writing – review & editing, Supervision, Conceptualization. **Andrej Šmuc:** Writing – review & editing, Methodology. **Primož Miklavc:** Writing – review & editing, Methodology. **Matej Dolenec:** Writing – review & editing, Methodology. **Matej Lipar:** Writing – original draft, Supervision, Investigation, Conceptualization.

Funding

This work was supported by the Slovenian Research and Innovation Agency basic research project and programs J6-50213, P6-0119, P6-0101, P6-0229, P1-0195 and I0-0031. The research was carried out whilst the senior author (MJ) was supported by the Slovenian Research and Innovation Agency Young Researcher programme MR-61263.

Declaration of competing interest

The authors declare that they have no known competing financial interests or personal relationships that could have appeared to influence the work reported in this paper.

Acknowledgements

We acknowledge and respect the Traditional Owners of the land in which we conducted our research.

Appendix A. Supplementary data

Supplementary data to this article can be found online at https://doi.org/10.1016/j.geomorph.2026.110414.

Data availability

The spatial dataset of shallow closed depressions generated in this study is openly available in the Zenodo repository. License: CC-BY 4.0. doi:https://doi.org/10.5281/zenodo.20182510.

References

Abeysinghe, P.B., 1998. Limestone and Limesand Resources of Western Australia. Geological Survey of Western Australia.

Agabi, C., 1995. Daya. In: Camps, G. (Ed.), Encyclopédie berbère: Daphnitae – Djado, vol. 15. National Book Centre, pp. 2246–2248.

Al-Halbouni, D., Watson, R.A., Holohan, E.P., Meyer, R., Polom, U., Dos Santos, F.M., Comas, X., Alrshdan, H., Krawczyk, C.M., Dahm, T., 2021. Dynamics of hydrological and geomorphological processes in evaporite karst at the eastern Dead Sea – a multidisciplinary study. Hydrol. Earth Syst. Sci. Discuss. 25 (6), 3351–3395. https://doi.org/10.5194/hess-25-3351-2021.

Alley, N.F., Clarke, J.D.A., Macphail, M., Truswell, E.M., 1999. Sedimentary innllings and development of major tertiary palaeodrainage systems of south-central Australia. In: Thiry, M., Simon-Coinçon, R. (Eds.), Palaeoweathering, Palaeosurfaces and Related Continental Deposits, pp. 337–366. https://doi.org/10.1002/9781444304190.ch14.

Australian Bureau of Statistics (ABS), 2021. Australia boundary [spatial data]. https://www.abs.gov.au/statistics/standards/australian-statistical-geography-standard-asgs-edition-3/jul2021-jun2026/access-and-downloads/digital-boundary-files.

Babikir, A.A.A., 1986. The vegetation of natural depressions in Qatar in relation to climate and soil. J. Arid Environ. 10 (3), 165–173. https://doi.org/10.1016/S0140-1963(18)31236-9.

Benbow, M.C., Alley, N.F., Callen, R.A., Greenwood, D.R., 1995. Geological history and palaeoclimate. In: Drexel, J.F., Preiss, W.V. (Eds.), The Geology of South Australia. Vol. 2, The Phanerozoic, vol. Bulletin(54). South Australia. Geological Survey, pp. 208–218.
Boas, T., Mallants, D., 2022. Episodic extreme rainfall events drive groundwater recharge in arid zone environments of central Australia. J. Hydrol. Reg. Stud. 40, 101005. https://doi.org/10.1016/j.ejrh.2022.101005.
Brooks, K.N., Ffolliott, P.F., Magner, J.A., 2013. Hydrology and the Management of Watersheds. John Wiley & Sons. https://doi.org/10.1002/9781118459751.
Bureau of Meteorology, 2006. Average annual, monthly and seasonal evaporation. Commonwealth of Australia. http://www.bom.gov.au/climate/maps/averages/evaporation/.
Bureau of Meteorology, 2024a. Average annual rainfall – 30 year climatology (1991–2020). https://www.bom.gov.au/climate/maps/averages/rainfall/.
Bureau of Meteorology, 2024b. Climate Data Online. https://www.bom.gov.au/climate/data/index.shtml.
Burnett, S., Webb, J.A., White, S., 2013. Shallow caves and blowholes on the Nullarbor Plain, Australia — flank margin caves on a low gradient limestone platform. Geomorphology 201, 246–253. https://doi.org/10.1016/j.geomorph.2013.06.024.
Burnett, S., Webb, J.A., White, S., Lipar, M., Ferk, M., Barham, M., O'Leary, M.J., Glover, F.S., 2020. Etched linear dunefields of the Nullarbor Plain; a record of Pliocene-Pleistocene wind patterns across southern Australia. Palaeogeogr. Palaeoclimatol. Palaeoecol. 557. https://doi.org/10.1016/j.palaeo.2020.109911.
Capot-Rey, R., 1939. Pays du Mzab et régions des Dayas. Etude sur le relief de la dorsale Saharienne. Ann. Géogr. 48 (271), 41–62.
Castellani, V., Dragoni, W., 1977. Surface Karst Landfroms on the Moroccan Hamada of Guir the 7th International Speleological Congress, England, Leicester.
Castellani, V., Dragoni, W., 1986. Evidence for karstic mechanisms involved in the evolution of Moroccan hamadas. Int. J. Speleol. 15, 57–71. https://doi.org/10.5038/1827-806X.15.1.5.
Clark, D., 2012. Neotectonic Features Database. https://pid.geoscience.gov.au/dataset/ga/74056.
Clarke, D.M., Mitchell, C.W., Varely, J.A., 1974. Geomorphic evolutin of sediment filled solution hollows in some arid regions (Northwestern Sahara). Z. Geomorphol. 20, 130–139.
Climate Engine, 2024. MNDWI [spatial data]. https://www.climateengine.org/.
Conrad, G., Geze, B., Paloc, H., 1967. Observations sur les phénomènes karstiques et pseudokarstiques du Sahara. Rev. Géogr. Phys. Géol. Dyn. 9 (5), 357–370.
De Waele, J., Gutiérrez, F., 2022. Karst Hydrogeology, Geomorphology and Caves. Wiley-Blackwell. https://doi.org/10.1002/9781119605379.
Delisser, E.A., 1865. Journal of Edmund A. Delisser. http://nla.gov.au/nla.obj-411378568.
Doerr, S.H., Davies, R.R., 2007. Combining remote sensing, geophysical and "old-school" geomorphological tools to assess weathering rates of the world's largest exposed carbonate platform: the Nullarbor Plain, Australia. In: GSA Denver Annual Meeting, USA, Denver.
EOC Geoservice, 2023. TanDEM-X 30m Edited DEM (EDEM) [spatial data]. https://geoservice.dlr.de/web/datasets/tdm30_edem.
ESRI, 2025. Satellite Imagery [Spatial Data].
Evans, I.S., 2012. Geomorphometry and landform mapping: what is a landform? Geomorphology 137 (1), 94–106. https://doi.org/10.1016/j.geomorph.2010.09.029.
Ford, D., Williams, P., 2007. Karst Hydrogeology and Geomorphology. John Wiley & Sons. https://doi.org/10.1002/9781118684986.
Gautier, M., 1951. Action eoliennes, phenomenes d'evaporation et d'hydrologie superficielle dans les regions aride. Centre national de la recherche scientifique.
Geoscience Australia, 2021. Radiometrics [spatial data]. https://www.ga.gov.au/scientific-topics/disciplines/geophysics/radiometrics.
Gillieson, D.S., Spate, A., 1992. The Nullarbor Karst. In: Gillieson, D.S. (Ed.), Geology, Climate, Hydrology and Karst Formation: Field Symposium in Australia; Guidebook, vol. Special Publication 4. Department of Geography and Oceanography, University College, Australian Defence Force Academy, pp. 65–99.
Gillieson, D.S., Cochrane, J.A., Murray, A., 1994. Surface hydrology and soil movement in an arid karst: the Nullarbor Plain, Australia. Environ. Geol. 23 (2), 125–133. https://doi.org/10.1007/bf00766986.
Goudie, A.S., 1991. Pans. Prog. Phys. Geogr. Earth Environ. 15 (3), 221–237. https://doi.org/10.1177/030913339101500301.
Goudie, A.S., 2004. Encyclopedia of Geomorphology. Routledge.
Goudie, A.S., 2010. Dayas: distribution and morphology of dryland solutional depressions developed in limestones. Z. Geomorphol. 54 (2), 145–159. https://doi.org/10.1127/0372-8854/2010/0054-0010.
Hocking, R.M., 1990. Eucla Basin. In: The Geology and Mineral Resources of Western Australia. Geological Survey of Western Australia, pp. 548–561.
Hou, B., Frakes, L.A., Sandiford, M., Worrall, L., Keeling, J., Alley, N.F., 2008. Cenozoic Eucla Basin and associated palaeovalleys, southern Australia — climatic and tectonic influences on landscape evolution, sedimentation and heavy mineral accumulation. Sediment. Geol. 203 (1–2), 112–130. https://doi.org/10.1016/j.sedgeo.2007.11.005.
James, N.P., Bone, Y., 1991. Origin of a cool-water, Oligo-Miocene deep shelf limestone, Eucla Platform, southern Australia. Sedimentology 38, 323–341.
James, N.P., Bone, Y., Carter, R.M., Murray-Wallace, C.V., 2006. Origin of the Late Neogene Roe Plains and their calcarenite veneer: implications for sedimentology and tectonics in the Great Australian Bight. Aust. J. Earth Sci. 53 (3), 407–419. https://doi.org/10.1080/08120090500499289.
Jennings, J.N., 1962. The limestone geomorphology of the Nullarbor Plains (Australia). In: Proceedings of the 2nd International Congress of Speleology.
Jennings, J.N., 1983. The disregarded karst of the arid and semiarid domain. Karstologia 1, 61–73.
Kokalj, Ž., Somrak, M., 2019. Why not a single image? Combining visualizations to facilitate fieldwork and on-screen mapping. Remote Sens. 11 (7). https://doi.org/10.3390/rs11070747.
Krapf, C., González-Álvarez, I., 2018. It is rather flat out there… regolith mapping depicting intricate landscape patterns and relationships to bedrock geology and structures under cover on the Nullarbor plain. In: Dutch, R., Wise, T., Pawley, M., Petts, M. (Eds.), Coompana Drilling and Geochemistry Workshop 2018 Extended Abstracts, vol. 19. Department for Energy and Mining, South Australia, Adelaide, pp. 12–17.
Lee, S., Irvine, D.J., Duvert, C., Rau, G.C., Cartwright, I., 2024. A high-resolution map of diffuse groundwater recharge rates for Australia. Hydrol. Earth Syst. Sci. 28 (7), 1771–1790. https://doi.org/10.5194/hess-28-1771-2024.
Li, Q., James, N.P., Bone, Y., McGowran, B., 1996. Foraminiferal biostratigraphy and depositional environments of the mid-Cenozoic Abrakurrie Limestone, Eucla Basin, southern Australia. Aust. J. Earth Sci. 43 (4), 437–450. https://doi.org/10.1080/08120099608728266.
Li, X.Y., Contreras, S., Solé-Benet, A., Cantón, Y., Domingo, F., Lázaro, R., Lin, H., Bas Van Wesemael, B., Puigdefábregas, J., 2011. Controls of infiltration–runoff processes in Mediterranean karst rangelands in SE Spain. Catena 86, 98–109. https://doi.org/10.1016/j.catena.2011.03.003.
Lipar, M., Ferk, M., 2015. Karst pocket valleys and their implications on Pliocene–Quaternary hydrology and climate: examples from the Nullarbor Plain, southern Australia. Earth-Sci. Rev. 150, 1–13. https://doi.org/10.1016/j.earscirev.2015.07.002.
Lowry, D.C., 1970. Geology of the Western Australian part of the Eucla Basin. Geol. Surv. West. Aust. Bull. 122, 1–200.
Lowry, D.C., Jennings, J.N., 1974. The Nullarbor karst, Australia. Z. Geomorphol. 18, 35–81.
Mabbutt, J.A., 1977. Desert Landforms. Australian National University Press.
Mazej, T., 2024. Geomorphological characteristics of cone karst in Slovenia University of Ljubljana. https://repozitorij.uni-lj.si/IzpisGradiva.php?lang=slv&id=161117.
Miller, C.R., James, N.P., Bone, Y., 2012. Prolonged carbonate diagenesis under an evolving late cenozoic climate; Nullarbor Plain, southern Australia. Sediment. Geol. 261-262, 33–49. https://doi.org/10.1016/j.sedgeo.2012.03.002.
Mitchell, C.W., 1970. The interpretation of dayas on aerial photographs. In: Berichte des III International en Symposiums fiir Photointerpretation, Germany, Dresden.
Mitchell, C.W., Willimott, S.G., 1974. Dayas of the Moroccan Sahara and other arid regions. Geogr. J. 140 (3), 441–453. https://doi.org/10.2307/1796537.
Moussaoui, T., Derdour, A., Benaradj, A., Hosni, A., 2024. Geomatic techniques for precise Dayas detection in arid zones: a case study in Northwestern Wilaya of Naama, Algeria. Euro-Mediterr. J. Environ. Integr. 9, 859–874. https://doi.org/10.1007/s41207-024-00477-4.
Novljan, Ž., 2021. Morphometry and density of dolines on slopes of Slovenian karst. Dela 56, 89–108. https://doi.org/10.4312/dela.56.89-108.
O'Connell, L.G., James, N.P., Bone, Y., 2012. The Miocene Nullarbor Limestone, southern Australia; deposition on a vast subtropical epeiric platform. Sediment. Geol. 253-254, 1–16. https://doi.org/10.1016/j.sedgeo.2011.12.002.
Oštir, K., 2006. Daljinsko zaznavanje. Inštitut za antropološke in prostorske študije ZRC SAZU. https://iaps.zrc-sazu.si/sites/default/files/9616568728.pdf.
Playford, P.E., Cope, R.N., Cockbain, A.E., Low, G.H., Lowry, D.C., 1975. Phanerozoic. In: Geology of Western Australia. West. Australia Geol. Survey, Mem, vol. 2, pp. 223–433.
Salomon, J.N., Pulina, M., 2005. Les karsts des régions climatiques extrêmes. Presses Universitaires de Bordeaux. https://doi.org/10.4000/books.pub.1064.
Sandiford, M., 2007. The tilting continent: a new constraint on the dynamic topographic field from Australia. Earth Planet. Sci. Lett. 261 (1–2), 152–163. https://doi.org/10.1016/j.epsl.2007.06.023.
Sellmann, S., Quigley, M., Duffy, B., Yang, H., Clark, D., 2022. Fault geometry and slip rates from the Nullarbor and Roe Plains of south-central Australia: insights into the spatial and temporal characteristics of intraplate seismicity. Earth Surf. Process. Landf. 48 (2), 350–370. https://doi.org/10.1002/esp.5490.
Shirani, K., Solhi, S., Pasandi, M., 2023. Automatic landform recognition, extraction, and classification using kernel pattern modeling. J. Geovis. Spat. Anal. 7 (2). https://doi.org/10.1007/s41651-022-00131-z.
Short, A.D., Tamura, T., Oliver, T.S.N., Detmar, S., Fotheringham, D., 2024. Quaternary clifftop and last glacial maximum dunes around the Great Australian Bight. Quat. Sci. Rev. 327, 108517. https://doi.org/10.1016/j.quascirev.2024.108517.
Smith, B., Mark, D.M., 2003. Do mountains exist? Towards an ontology of landforms. Environ. Plan. B Urban Analytics City Sci. 30 (3), 411–427. https://doi.org/10.1068/b12821.
Sniderman, J.M.K., Woodhead, J.D., Hellstrom, J., Jordan, G.J., Drysdale, R.N., Tyler, J. J., Porch, N., 2016. Pliocene reversal of late Neogene aridification. Proc. Natl. Acad. Sci. USA 113 (8), 1999–2004. https://doi.org/10.1073/pnas.1520188113.
Stefanovski, S., Kokalj, Ž., Stepišnik, U., 2024. Sky-view factor enhanced doline delineation: a comparative methodological review based on case studies in Slovenia. Geomorphology 465. https://doi.org/10.1016/j.geomorph.2024.109389.
Stewart, A.J., Sweet, I.P., Needham, R.S., Raymond, O.L., Whitaker, A.J., Liu, S.F., Phillips, D., Retter, A.J., Connolly, D.P., Stewart, G., 2008. Surface Geology of Australia 1:1,000,000 Scale, Western Australia [Spatial Data]. The Commonwealth of Australia, Geoscience Australia, Canberra.
Stone, J., Allan, G.L., Fifield, L.K., Evans, J.M., Chivas, A.R., 1994. Limestone erosion measurements with cosmogenic chlorine-36 in calcite — preliminary results from Australia. Nucl. Instrum. Methods Phys. Res., Sect. B 92 (1–4), 311–316. https://doi.org/10.1016/0168-583x(94)96025-9.

Suharyanto, D., Suhartanto, E., Lesmana, S.B., 2020. Watershed morphometric classification analysis using geographic information system. Int. J. Geomate. 19 (74), 114–122. https://geomatejournal.com/geomate/article/view/1856.

Tanh, L., 2021. Quantifying and Modeling the Surficial Karst of the Nullarbor Plain (Southern Australia) University of Miami. Coral Gables, Florida.

Thiéry, A., 1991. Multispecies coexistence of branchiopods (Anostraca, Notostraca & Spinicaudata) in temporary ponds of Chaouia plain (western Morocco): sympatry or syntopy between usually allopatric species. Hydrobiologia 212, 117–136.

van der Meij, W.M., Meijles, E.W., Marcos, D., Harkema, T.T.L., Candel, J.H.J., Maas, G. J., 2021. Comparing geomorphological maps made manually and by deep learning. Earth Surf. Process. Landf. 47 (4), 1089–1107. https://doi.org/10.1002/esp.5305.

Veress, M., 2017. Solution doline development on glaciokarst in alpine and Dinaric areas. Earth Sci. Rev. 173, 31–48. https://doi.org/10.1016/j.earscirev.2017.08.006.

Veress, M., Méhes, E., 2021. Climate change and karst systems: an overview. Geosciences 11 (12), 513. https://doi.org/10.3390/geosciences11120513.

Wakelin-King, G.A., Webb, J.A., 2020. Origin, geomorphology and geoheritage potential of Australia's longest coastal cliff lines. Aust. J. Earth Sci. 67 (5), 649–661. https://doi.org/10.1080/08120099.2020.1742202.

Webb, J.A., James, J.M., 2023. Nullarbor. In: Webb, J.A., White, S., Smith, G.K. (Eds.), Australian Caves and Karst Systems. Springer, pp. 171–187. https://doi.org/10.1007/978-3-031-24267-0_11.

Webb, J.A., White, S.Q., 2013. Karst in deserts. In: Shroder, J.F., Frumkin, A. (Eds.), Treatise on Geomorphology. Academic Press, pp. 171–187.

Webb, J.A., Grimes, K.G., Osborne, A., 2003. Black holes: caves in the Australian landscape. In: Finlayson, B.L., Hamilton-Smith, E. (Eds.), Beneath the Surface: A Natural History of Australian Caves. University of New South Wales Press, pp. 1–52.

Wessel, B., 2018. TanDEM-X Ground Segment – DEM products specification document (public document TD-GS-PS-0021, issue 3.2). http://refhub.elsevier.com/S0031-0182(20)30356-4/rf0095.

Wickens, G.E., 1998. Arid and semi-arid environments of the world. In: Ecophysiology of Economic Plants in Arid and Semi-arid Lands. Springer, pp. 5–15. https://doi.org/10.1007/978-3-662-03700-3_2.

Wilson, J.P., Gallant, J.C., 2000. Terrain Analysis: Principles and Applications. John Wiley & Sons.

Woodhead, J., Sniderman, J.M.K., Hellstrom, J., Drysdale, R.N., Maas, R., White, N., White, S., Devine, P., 2019. The antiquity of Nullarbor speleothems and implications for karst palaeoclimate archives. Sci. Rep. 9, 603. https://doi.org/10.1038/s41598-018-37097-2.

Xu, H., 2006. Modification of normalised difference water index (NDWI) to enhance open water features in remotely sensed imagery. Int. J. Remote Sens. 27 (14), 3025–3033. https://doi.org/10.1080/01431160600589179.